Atypical B cells consist of subsets with distinct effector functions

Raphael A. Reyes[1†], Gayani Batugedara[1†], Paramita Dutta[2], Ashley B. Reers[1], Rolando Garza[1], Isaac Ssewanyana[3,4], Prasanna Jagannathan[5,6], Margaret E. Feeney[7,8], Bryan Greenhouse[7], Sebastiaan Bol[1], Ferhat Ay[2,9], Evelien M. Bunnik[1*]

[1] Department of Microbiology, Immunology and Molecular Genetics, Long School of Medicine, The University of Texas Health Science Center at San Antonio, San Antonio, TX, USA
[2] Division of Vaccine Discovery, La Jolla Institute for Immunology, La Jolla, CA, USA
[3] Infectious Disease Research Collaboration, Kampala, Uganda
[4] Department of Infection Biology, London School of Hygiene and Tropical Medicine, London, United Kingdom
[5] Department of Medicine, Division of Infectious Diseases, Stanford University, Stanford, CA, USA
[6] Department of Microbiology and Immunology, Stanford University, Stanford, CA, USA
[7] Department of Medicine, University of California, San Francisco, CA, USA
[8] Department of Pediatrics, University of California, San Francisco, CA, USA
[9] School of Medicine, University of California San Diego, La Jolla, CA, USA

*Corresponding author. Email: bunnik@uthscsa.edu

[†] These authors contributed equally to this work

Abstract

Atypical B cells are a population of activated B cells that are commonly enriched in individuals with chronic immune activation, but are also part of a normal immune response to infection or vaccination. Prior studies to determine the function of these cells have yielded conflicting results, possibly due to functional heterogeneity among this B cell population. To better define the role(s) of atypical B cells in the host adaptive immune response, we performed single-cell sequencing of transcriptomes, cell surface markers, and B cell receptors in individuals with chronic *Plasmodium falciparum* exposure, a condition known to lead to accumulation of circulating atypical B cells. Our studies identified three previously uncharacterized populations of atypical B cells with distinct transcriptional and functional profiles, that separate into two differentiation pathways. We identified a set of cell surface markers to distinguish these atypical B cell subsets and confirmed their presence in malaria-experienced children and adults using flow cytometry. *Plasmodium falciparum*-specific cells were present in equal proportions within each of these atypical B cell populations, indicating that all three subsets develop in response to antigen stimulation. However, we observed marked differences among the three subsets in their ability to produce IgG upon T-cell-dependent activation. Collectively, our findings help explain the conflicting observations in prior studies on the functions of atypical B cells and provide a better understanding of their role in the adaptive immune response in chronic inflammatory conditions.

One sentence summary

Atypical B cells consist of three subsets that may play distinct roles in the host adaptive immune response.

48 **INTRODUCTION**

49 Humoral immunity to infection relies on the development of memory B cells that circulate through
50 the blood and secondary lymphoid organs to patrol for antigen, as well as long-lived plasma cells
51 that home to the bone marrow and function as a source of antibodies that inhibit pathogen
52 replication and survival. In humans, memory B cells are defined based on the expression of the
53 surface proteins CD21 and CD27. Upon vaccination or acute infection, other antigen-experienced
54 B cell populations transiently increase in abundance in the circulation, including $CD21^{-}CD27^{+}$
55 activated B cells and $CD21^{-}CD27^{-}$ atypical B cells (also called DN2 cells) (*1-3*). These activated
56 and atypical B cell populations are thought to be part of a normal immune response and peak in
57 abundance within 2 to 4 weeks after antigen exposure, followed by a gradual return to baseline
58 over the course of several months (*1, 4*). However, under conditions of chronic or repetitive
59 immune activation, as seen during HIV or *Plasmodium* infection, and in autoimmune diseases,
60 such as systemic lupus erythematosus (SLE), atypical B cells accumulate and become a more
61 prominent presence in the circulation (*5-8*). In healthy adults, atypical B cells make up
62 approximately 2 - 4% of all circulating B cells, but this can increase to 20 – 40% in individuals with
63 chronic inflammatory conditions (*5, 6, 9*). Whether these atypical B cells contribute to control of
64 infections or negatively affect the host immune response remains incompletely understood. A
65 better understanding of the function of atypical B cells will provide insight into the immune
66 response to chronic infection and may present ways to overcome immune dysfunction or to
67 harness these cells by vaccination.

68 Studies regarding the functionality of atypical B cells in the immune response have highlighted
69 various differences between atypical B cells and memory B cells. Specifically, atypical B cells
70 display reduced expression of B cell receptor signaling pathway genes and costimulatory
71 molecules, as well as upregulation of inhibitory receptors (*10, 11*). In addition, atypical B cells
72 were less responsive to B cell receptor engagement by soluble antigen and showed reduced

73 differentiation into antibody-secreting cells under conditions that efficiently induced differentiation
74 of memory B cells into antibody-secreting cells (*5, 8-10, 12*). These results initially led to the
75 conclusion that atypical B cells are exhausted and non-responsive to stimulation. However, it was
76 recently reported that atypical B cells respond robustly to high-affinity membrane-associated
77 antigen and showed a markedly reduced response to low-affinity antigens, a selective mechanism
78 which may serve to limit activation of atypical B cells by low-affinity antigens, such as auto-
79 antigens (*11, 13*). Despite these new findings, the contribution of atypical B cells to the host
80 immune response remains subject of debate and various functions have been proposed for these
81 cells. These include (pre-)antibody secreting cells, based on the presence of secretory Ig
82 transcripts and the overlap in B cell receptor sequences between atypical B cells and plasma
83 cells, and immune-modulatory cells, based on the upregulation of surface proteins that promote
84 interactions between B cells and T cells (*9, 11, 14-18*). The multiple and conflicting effector
85 functions previously assigned to atypical B cells are suggestive of functional heterogeneity among
86 this population.

87 Here, we used chronic *P. falciparum* exposure as a model to define the heterogeneity of the
88 atypical B cell compartment. Over the course of many years of repetitive *P. falciparum* infections,
89 people living in malaria-endemic regions develop an immune response that protects against
90 disease. As a result, most cases of malaria occur in children under the age of 10, while adults
91 with life-long exposure have asymptomatic infections. To study atypical B cells induced by
92 malaria, we performed single-cell transcriptomic analysis with cell surface marker and B cell
93 receptor profiling on longitudinal samples obtained from two children following malaria. Based on
94 these sequencing data, we defined three subsets of atypical B cells with distinct transcriptional
95 profiles that are likely to play different roles in the immune response. Using flow cytometry, we
96 then analyzed the longevity and *Plasmodium* antigen-specificity among these subsets in samples
97 from malaria-experienced children and adults.

98

99 **RESULTS**

100 **Single-cell transcriptomics identifies B cell populations**

101 The atypical B cell population is strongly expanded in the first few weeks after a malaria episode
102 and slowly contracts to baseline levels over the course of several months (*4*). To study the
103 identity of atypical B cells induced as a result of the hyperinflammatory immune response during
104 malaria and following return to baseline conditions, we selected two children (5 and 7 years old)
105 for whom peripheral blood mononuclear cell (PBMC) samples were collected three weeks after
106 malaria and six months later (**Figure 1A**, **Table S1**). Both children were free of symptomatic
107 malaria between the two time points, but had detectable *P. falciparum* parasitemia at both the
108 three- and six-month time points (**Figure S1**). Asymptomatic *P. falciparum* infections result in
109 very low immune activation (*19*), and it can therefore be expected that the atypical B cell
110 population is only minimally affected by these infections, especially in comparison to the strong
111 inflammatory response during malaria.

112 We first isolated naïve and antigen-experienced B cells by fluorescence-activated cell sorting
113 based on the expression of CD21 and CD27 (**Figure 1B**). Naïve B cells typically make up a
114 large fraction of the total B cell pool (43 – 60% in the samples used here), but are not of interest
115 when studying the response of B cells to infection. Therefore, we enriched our samples for
116 antigen-experienced B cells, but added in some naïve B cells to have representation of all B cell
117 populations in the final cell pool. (**Table S2**). Each sample was then subjected to single-cell
118 RNA-sequencing in combination with analysis of select cell surface marker expression and B
119 cell receptor-sequencing on the 10x Genomics platform. Cells that passed quality control (n =
120 21,439; **Table S3**) were clustered into eleven populations based on gene expression and
121 visualized by Uniform Manifold Approximation and Projection (UMAP) (**Figure 1C**). UMAP

122

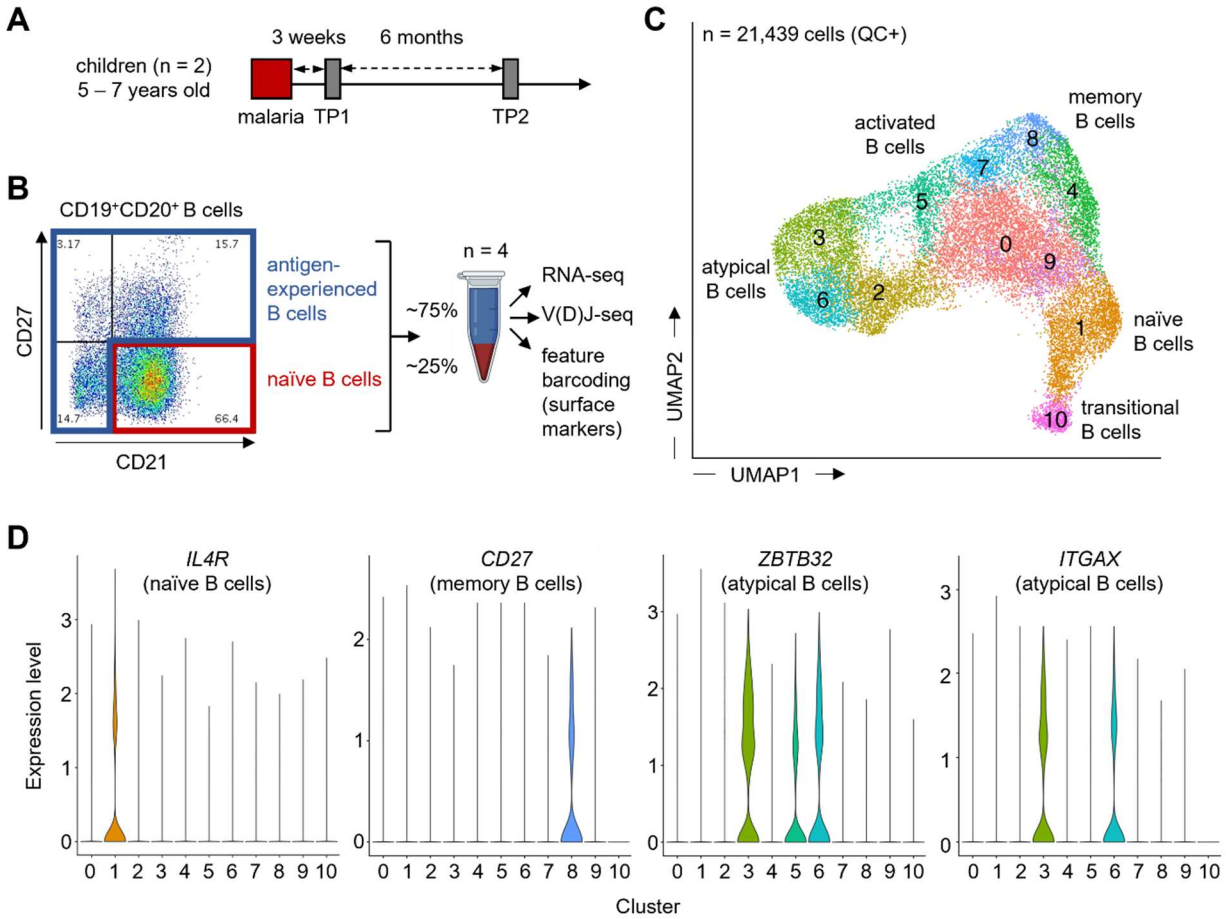

Figure 1: Single-cell sequencing of B cells in malaria-experienced children. A) Timeline of sample collection at three weeks post-malaria (TP1) and six months later (TP2) in two children. Children did not experience malaria between the first and second sample collection. **B)** Flow cytometry strategy to enrich for antigen-experienced B cells. A majority of antigen-experienced B cells were mixed with naïve B cells and used for library preparation using the 10x Genomics platform. This yielded three different libraries for each sample to study gene expression, V(D)J sequences, and cell surface marker expression in the same cells. **C)** UMAP of all B cells that passed quality control (QC+), showing 11 transcriptomic B cell clusters. Major subsets identified based on the expression of key genes and previously published gene signatures are indicated. **D)** Expression levels of genes characteristic for naïve B cells (*IL4R*), memory B cells (*CD27*), and atypical B cells (*ZBTB32* and *ITGAX*). TP, time point.

136 visualizes cell clusters in a 2D plot based on similarity in transcriptional profile. Each of the four
137 samples was well represented in all eleven clusters (**Figure S2; Table S4**). Notably,
138 immunoglobulin-related genes were excluded during clustering to prevent antibody isotype or
139 V(D)J-gene segment usage from influencing these results, as was previously proposed by
140 Stewart *et al*. (*20*). Comparing the expression levels of individual key genes (**Figure 1D**), as well
141 as gene signatures of various B cell populations generated by others (**Figure S3**) (*11, 20, 21*),
142 allowed us to identify the location of major B cell populations in the UMAP. This included
143 transitional B cells in cluster 10, naive B cells (expressing *IL4R*) in cluster 1, and memory B cells
144 (expressing *CD27*) in cluster 8. In total, 83% of all cells in our data set were found in clusters
145 with a non-naive transcriptional signature, confirming that our data set was enriched for antigen-
146 experienced cells. Clusters 3, 5, and 6 expressed genes associated with atypical B cells, such
147 as *ZBTB32*, encoding a transcription factor, and *ITGAX,* encoding the surface protein CD11c
148 (**Figure 1D**). Together, these two clusters represented almost 30% of all data (6,088 cells),
149 making this a rich dataset to study heterogeneity among atypical B cells in malaria-experienced
150 individuals.

151

152 **Phenotypically defined atypical B cells have multiple distinct transcriptomic profiles**

153 We next sought to determine how well the atypical B cell clusters that we identified based on
154 transcriptomic profiles corresponded to $CD21^{-}CD27^{-}$ B cells, which is the phenotypic
155 classification for atypical B cells most commonly used in the malaria field. We therefore used
156 cell surface markers CD21 and CD27 to 'gate' cells, similar to how this is commonly done in
157 flow cytometry (**Figure S4**). Nearly all cells in clusters 3 and 6 were $CD21^{-}CD27^{-}$, in agreement
158 with their transcriptomic profile of atypical B cells (**Figure 2A, Figure S5**). However, $CD21^{-}$
159 $CD27^{-}$ B cells also made up about 50% of cluster 5. Cluster 10 was also comprised of

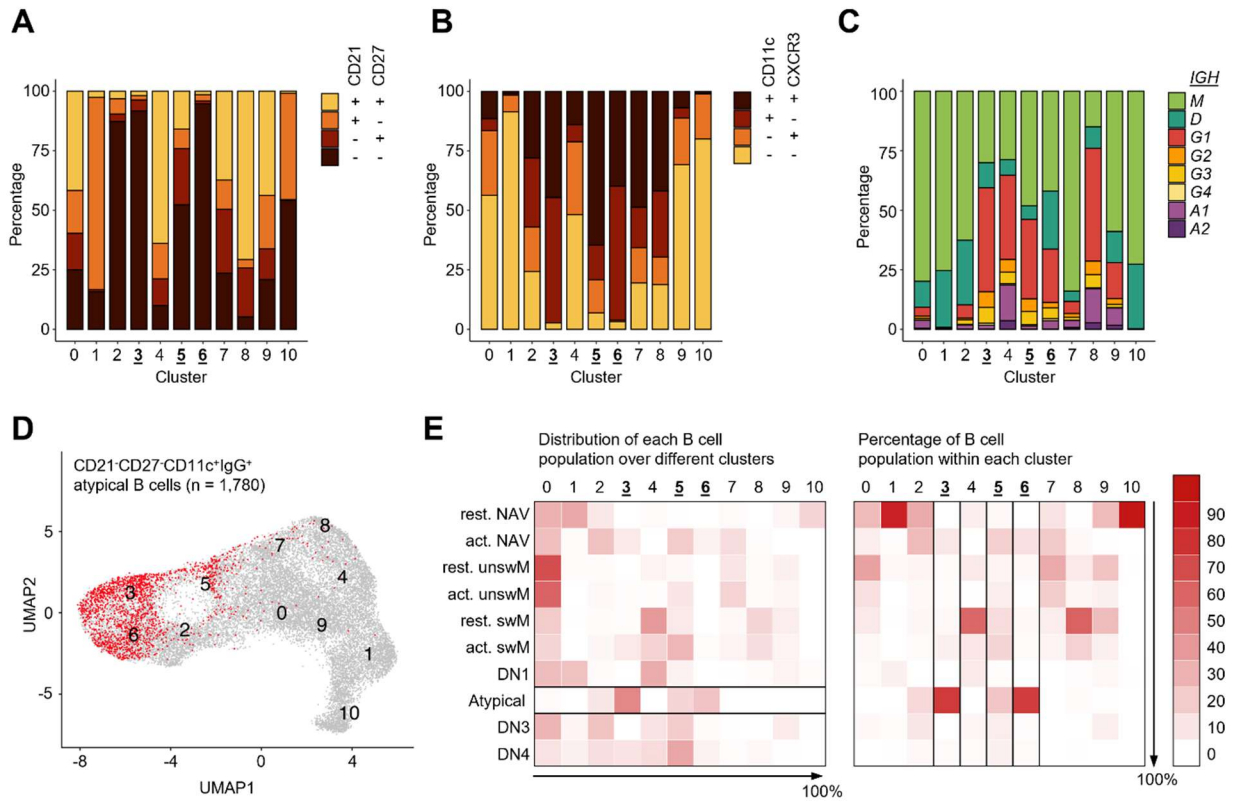

Figure 2: Phenotypically defined atypical B cells are found in three transcriptionally distinct clusters. A) Distribution of CD21$^{-/+}$ CD27$^{-/+}$ B cells among all transcriptional clusters. **B)** Distribution of CD11c$^{-/+}$ CXCR3$^{-/+}$ B cells among all transcriptional clusters. **C)** Distribution of immunoglobulin heavy chain transcripts among all transcriptional clusters. **D)** Projection of phenotypically defined atypical B cells (shown in red) onto the transcriptomics-based UMAP. All non-atypical B cells are shown in gray. **E)** The distribution of each B cell population over the different clusters (left) and the percentage of phenotypically defined B cell populations within each cluster (right). The direction in which the values in the rows (left) or columns (right) add up to 100% is indicated with an arrow. The atypical B cell population (left heatmap) and clusters 3, 5, and 6 (right heatmap) mentioned in the text are highlighted with borders. Rest., resting; act., activated; NAV, naïve, unswM, unswitched memory; swM, switched memory; DN, double negative.

174 approximately 50% CD21$^-$CD27$^-$ cells, which were transitional B cells that have recently
175 emigrated from the bone marrow and have yet to upregulate CD21 expression (**Figure S3A**).
176 Additionally, cluster 2 largely consisted of CD21$^-$CD27$^-$ cells that had not undergone class
177 switching (see also below). The CD21$^-$CD27$^-$ cells in clusters 2 and 10 were therefore excluded
178 from our analysis. In a recent study by Sutton *et al.*, atypical B cells were observed to
179 predominantly express CD11c and CXCR3 (*3*). We therefore also analyzed the distribution of
180 CD11c$^{+/-}$ CXCR3$^{+/-}$ populations among the nine B cell clusters (**Figure S6**). The large majority of
181 cells in clusters 3 and 6 expressed CD11c (75% and 98%, respectively), while expression of
182 CXCR3 was observed in only ~45% of all cells in these clusters (**Figure 2B, Figure S5**). In
183 contrast, 79% of cells in cluster 5 were CXCR3$^+$, most of which also expressed CD11c. These
184 percentages were similar when limiting the analysis to CD21$^-$CD27$^-$ B cells (**Figure S7**). These
185 data suggest that CXCR3 marks a subset of atypical B cells but cannot be used as a marker to
186 identify all atypical B cells. Next, we analyzed the heavy chain sequences from the B cell
187 receptor-sequencing libraries to determine isotype usage among the different clusters. This
188 analysis showed that, as expected, the transitional cells in cluster 10 and naïve B cells in cluster
189 1 were unswitched cells, expressing only *IGHM* and *IGHD*. Atypical B cell clusters 3, 5, and 6
190 contained larger fractions of class-switched B cells (**Figure 2C, Figure S5**). Cluster 3 in
191 particular showed a distribution of *IGH* transcripts approaching that of cluster 8 memory B cells,
192 with the exception of a lack of *IGHA1* expression, suggesting that cluster 3 atypical B cells have
193 undergone class-switch recombination at similar rates as memory B cells.

194 To further delineate the distribution of different B cell populations among our transcriptomic
195 clusters, we identified B cells by phenotype based on the surface expression of CD21, CD27,
196 CD11c, IgM, and IgG following recently published guidelines (*22*). Because our cell surface
197 marker analysis did not include IgD, we made two exceptions to these guidelines. First,
198 unswitched B cells were not identified based on the presence of IgD but that of IgM, which is

199 usually co-expressed with IgD. Second, switched B cells were identified based on the presence
200 of IgG instead of the absence of IgD, isotypes that are mutually exclusive. We first used CD27
201 and IgM or IgG expression to distinguish naive B cells (NAV, $CD27^-IgM^+$), unswitched memory B
202 cells (unswM, $CD27^+IgM^+$), and switched memory B cells (swM, $CD27^+IgG^+$). These populations
203 were further divided into resting ($CD21^+$) and activated ($CD21^-$). The majority of resting switched
204 memory B cells were located in clusters 0, 4, and 8. We also identified DN B cells ($CD27^-IgG^+$),
205 which were divided into DN1 ($CD21^+CD11c^-$), DN2 ($CD21^-CD11c^+$), DN3 ($CD21^-CD11c^-$), and
206 DN4 ($CD21^+CD11c^+$) (**Figure S8**). IgM^+ atypical B cells are also known as activated naive B
207 cells, and IgG^+ atypical B cells are equivalent to DN2 B cells. We recently reported substantial
208 differences in intrinsic properties between IgM^+ and IgG^+ atypical B cells that are likely related to
209 their origin and function (*23*). Additionally, CD11c has been identified as the marker that best
210 delineates atypical B cells (*3, 24*). We therefore decided to use the phenotypic definition of DN2
211 B cells to identify atypical B cells for the remainder of this study: $CD21^-CD27^-IgG^+CD11c^+$
212 (**Figure 2D**). Of all phenotypically defined atypical B cells, 47% were found in cluster 3, 23% in
213 cluster 6, and 17% in cluster 5 (**Figure 2E**). The majority of cells in cluster 3 (77%) and cluster 6
214 (75%) were atypical B cells (**Figure 2E**). Cluster 5 was more diverse with 23% atypical B cells,
215 19% activated naïve B cells, 13% resting switched memory B cells, 16% activated switched
216 memory B cells, and 29% other B cell populations. Of note, clusters 3, 5, and 6 were stable at a
217 clustering resolution ≥ 0.6. At a clustering resolution below 0.6, cluster 6 was merged with
218 cluster 2 that predominantly contained activated naïve B cells (**Figure S9**). For this reason, a
219 resolution of 0.6 was chosen for the analysis presented here. Collectively, these results show
220 that phenotypically defined class-switched atypical B cells in malaria-experienced children
221 consist of multiple distinct subsets with unique transcriptional profiles.

222

223 **Differences in gene expression programs of atypical B cells are associated with different**
224 **roles in the immune response**

225 To better understand the identity of the three subsets of atypical B cells identified in this study
226 found in clusters 3, 5, and 6, we compared the expression of genes that have previously been
227 described as part of the unique transcriptional profile of atypical B cells (*10-12*). The up or down
228 regulation of various genes in these clusters as compared to resting switched memory B cells in
229 cluster 8 was consistent with previous reports (**Figure 3A**). Two manuscripts recently posted on
230 bioRxiv showed that the transcription factor *ZEB2* acts as an important regulator for the
231 development of atypical B cells (*25, 26*). ZEB2 was also expressed significantly higher in
232 clusters 3, 5, and 6 as compared to cluster 8 (**Figure 3A**). In contrast, several atypical B cell-
233 associated genes were uniquely expressed in only one of the three clusters (**Figure 3B**). For
234 example, the integrin-encoding genes *ITGB2* and *ITGB7* were predominantly expressed in
235 cluster 3. In contrast, *CD72*, encoding a surface marker that inhibits B cell responses and
236 prevents antibody production (*27*), was more abundantly expressed in cluster 6. *CXCR3*
237 expression was highest in cluster 5, in line with the results of the cell surface marker analysis
238 (**Figure 2B**). These differences in gene expression highlight that bulk atypical B cells are a
239 mixture of various subsets and point to functional differences in activation status and the
240 potential for cell-cell interactions between these subsets.

241 To gain insight into potential differences in function between cells in clusters 3, 5, and 6, we
242 performed Reactome pathway analysis using genes that were upregulated or downregulated in
243 pair-wise comparisons of the three clusters (**Figure 3C-D, Tables S5 – S6**). Atypical B cells in
244 cluster 6 showed higher expression of 8 out of 99 genes encoding ribosomal proteins (for
245 example, *RPS8*, *RPS18*, and *RPS19*) and were most strongly enriched for pathways related to
246 translation. Ribosomal genes were also highly expressed in cluster 8 switched memory B cells,
247 suggesting that this may be a feature of cells poised to undergo cell differentiation. Atypical B

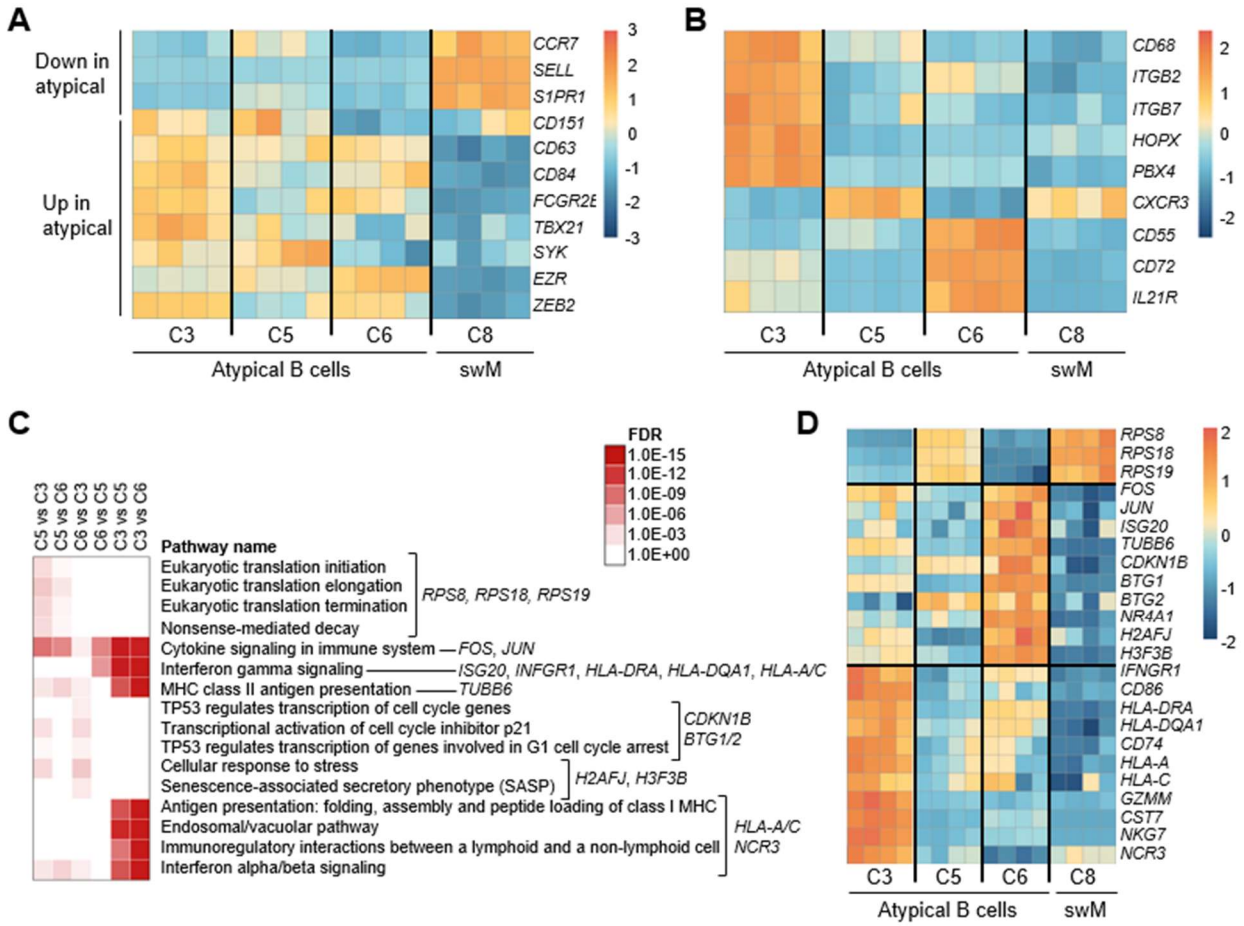

Figure 3: Phenotypic and functional differences between subsets of atypical B cells. A) Expression of genes previously identified as part of the unique transcriptional signature of atypical B cells that are consistently expressed higher or lower in all three subsets of atypical B cells as compared to class-switched resting memory B cells (swM; cluster 3). **B)** Differential expression of atypical B cell-associated genes between the three subsets of atypical B cells. **C)** Selected reactome pathways that were significantly enriched (FDR-corrected P value < 10^{-4}) in pair-wise comparisons between the three clusters that contain atypical B cells. Key differentially expressed genes in these pathways that are shown in panel D are indicated. **D)** Select differentially expressed genes in atypical B cell clusters that were present in enriched Reactome pathways and are discussed in the text. The four columns represent the four samples subjected to scRNA-seq analysis. C8, cluster 8; C3, cluster 3; C5, cluster 5; C6, cluster 6

261 cells in both clusters 3 and 6 upregulated genes in response to stimulation by interferon gamma
262 and cytokines, but the outcome of this response differed between the two clusters. Atypical B
263 cells in cluster 6 upregulated genes encoding components of the Activator Protein 1 (AP1)
264 complex, including *FOS* and *JUN*, as well as interferon-stimulated genes (for example, *ISG20*),
265 and tubulin genes (for example, *TUBB6*). Additionally, cluster 6 atypical B cells were enriched
266 for pathways that signified negative regulation of cell cycle progression. Upregulated genes
267 included the cyclin-dependent kinase inhibitor *CDKN1B*, the anti-proliferative genes *BTG1/2*,
268 and the transcriptional repressor *NR4A1*. Nuclear receptor 4A1 is part of a family of transcription
269 factors that was recently implicated in a negative feedback loop that rendered B cells more
270 dependent on T cell help and promoted peripheral B cell tolerance (*28, 29*). Finally, cluster 6
271 atypical B cells showed increased expression of variant histones, associated with a pro-
272 inflammatory stress response resulting in cellular senescence (*30*)(*31, 32*). The transcriptional
273 profile of atypical B cells in cluster 6 thus pointed to an interferon-driven response that resulted
274 in senescence or anergy. On the other hand, atypical B cells in cluster 3 were enriched for
275 pathways related to antigen processing and presentation, and immunoregulation. Among the
276 genes upregulated in cluster 3 were genes encoding proteins that promote interactions between
277 B cells and T cells, such as HLA-DR/DQ, CD86, which is downregulated by NR4A1, and CD74,
278 which regulates antigen presentation by class II MHC (*33-35*). In addition, we observed
279 upregulation of genes encoding class I MHC (*HLA-A* and *HLA-C*) and several genes that are
280 associated with cytotoxicity, including granzyme M (*GZMM*), cystatin 7 (*CST7*), natural killer cell
281 granule protein 7 (*NKG7*, a target gene of T-bet), and natural cytotoxicity triggering receptor 3
282 (*NCR3*). This gene signature suggests that these cells have increased exocytosis activity, which
283 could affect cell-cell interactions and have an immunomodulatory function. Collectively, our
284 results indicate that phenotypically defined IgG^+ atypical B cells can have one of three different
285 transcriptional profiles that are associated with different functions within the immune response.

286 **Atypical B cells form two separate compartments**

287 To study the development of the different subsets of atypical B cells, we turned to an analysis of
288 their B cell receptor sequences. We first assessed the amount of affinity maturation each B cell
289 population has undergone by determining the level of somatic hypermutation in each cluster.
290 This revealed that clusters 3 and 5 on average accumulated similar levels of mutations as class-
291 switched memory B cells in cluster 8, while the average mutation frequency in cluster 6 was
292 more than 50% lower (**Figure 4A, Figure S10A**). However, this may in part be caused by the
293 larger fractions of unswitched B cells in cluster 6 (**Figure 2C**). When including only class-
294 switched atypical B cells, we still observed a higher average level of somatic hypermutation in
295 clusters 3 and 5 than in cluster 6, although the difference was slightly smaller (**Figure 4B,**
296 **Figure S10B**). This difference suggests that cluster 6 atypical B cells have not undergone
297 extensive affinity maturation and seem to be more closely related to naïve B cells. Atypical B
298 cells in clusters 3 and 5 have undergone similar levels of affinity maturation as memory B cells,
299 which could indicate that they are derived from memory B cells or have a similar developmental
300 trajectory. However, while somatic hypermutation and affinity maturation typically occur inside
301 germinal centers, these processes can also occur in extrafollicular sites (*36*) and our results are
302 therefore not direct evidence for the developmental pathway of atypical B cells.

303 Next, we wished to better understand the developmental relationship between the three
304 subsets. To this end, we first employed RNA velocity analysis to infer the developmental
305 trajectories of the three atypical B cell subsets. This analysis uses the ratio of unspliced and
306 spliced transcripts to identify genes that undergo upregulation (more unspliced than spliced
307 transcripts) or downregulation (more spliced than unspliced transcripts). These transcript
308 dynamics are then used to model the direction and speed of movement of individual cells (*37*).
309 This analysis revealed two dominant developmental trajectories: (1) cluster 6 atypical B cells
310 were mainly derived from activated naïve B cells in cluster 2 and did not develop further, while

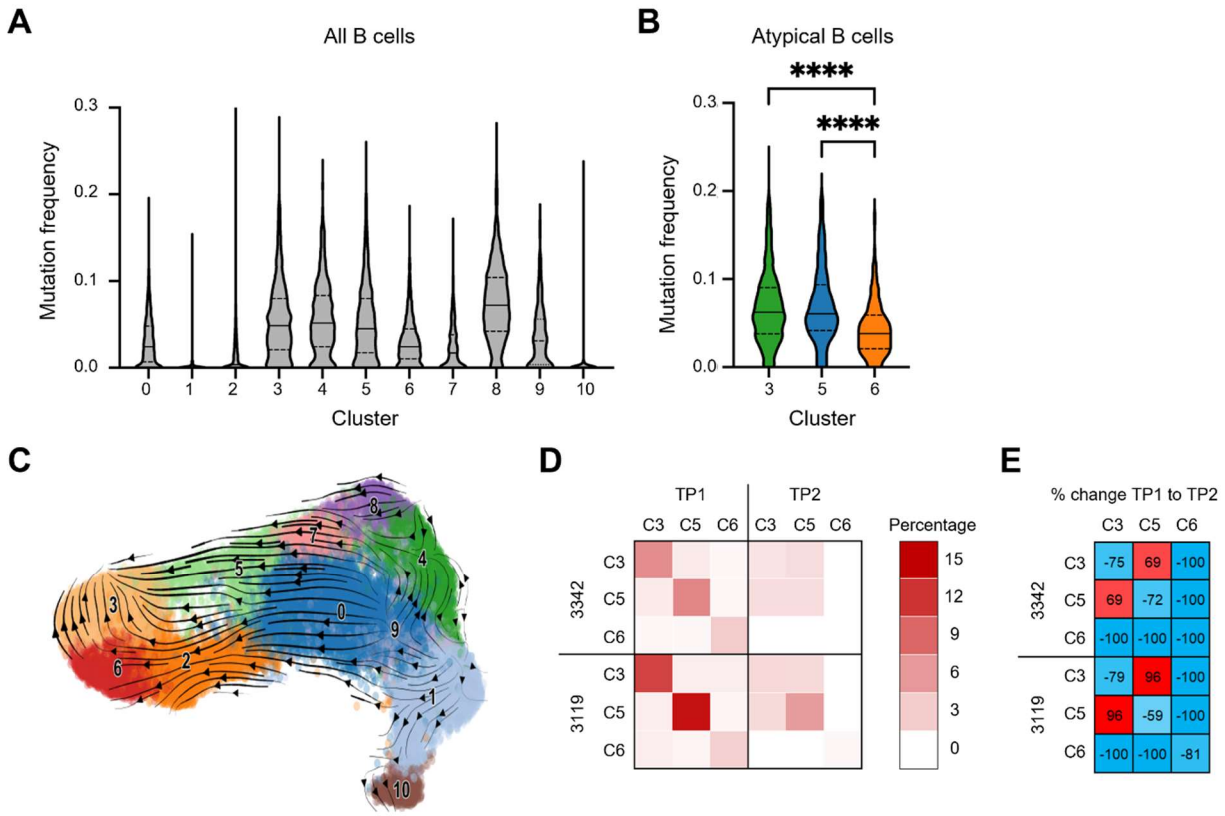

Figure 4: Developmental relationships between atypical B cell subsets. A) Levels of somatic hypermutation among the transcriptomics-based B cell clusters. **B)** Levels of somatic hypermutation among phenotypically defined atypical B cells in clusters 3, 5, and 6. In panels A and B, the median is shown as a solid horizontal lines, while the quartiles are represented by dashed horizontal lines. In panel B, a one-way ANOVA was used to test for statistically significant differences between the groups. P values shown are from Tukey's post hoc test. **** $P < 0.0001$. **C)** Analysis of the developmental trajectory of B cells using scVelo. **D)** Clonal expansion within clusters (along the diagonal in each quadrant of the heatmap) and clonal connections between clusters (off-diagonal cells) for the three clusters that contain atypical B cells at 3 weeks post-malaria (TP1) and six months later (TP2). **E)** The percentage change in clonal expansion/connections between the first and the second time point for the three clusters that contain atypical B cells. TP, time point

325 (2) cluster 3 atypical B cells seemed to be predominantly derived from memory B cells, with
326 cluster 5 atypical B cells as an intermediate step in this trajectory (**Figure 4C**). To confirm these
327 developmental connections between the atypical B cell subsets, we calculated the level of
328 expansion of clonal B cell lineages within each cluster at the two time points, as well as the
329 percentage of clonal connections between clusters, as described in more detail previously (*38*).
330 B cells were considered part of the same lineage when their heavy chain variable region
331 contained the same *IGHV* and *IGHJ* genes, and shared at least 85% amino acid sequence
332 identity in the heavy chain (H) CDR3 (*39, 40*). In all three atypical B cell clusters, there was
333 strong expansion of B cells at 3 weeks post-malaria, with 3 – 14% of B cells within each cluster
334 belonging to the same lineage (**Figure 4D, Figure S11A**). This was followed by contraction six
335 months later, resulting in a loss of more than 50% of clonal lineages (**Figure 4D, E**). This
336 contraction points to a return to a resting state and suggests that minimal immune activation
337 occurred as a result of the asymptomatic infection at 6-months post-malaria, as compared to the
338 strong immune response elicited by malaria. At 3 weeks post-malaria, 0.5 – 1.0% of clonal
339 sharing occurred between cluster 6 and clusters 3/5, but these connections were completely lost
340 six months later. In contrast, the connectivity between cluster 3 and cluster 5 increased at the
341 second time point, as compared to the time point shortly after malaria, and this was the only pair
342 of clusters for which this happened consistently (**Figure 4E, Figure S11B**). These observations
343 suggest that cluster 6 atypical B cells form a separate compartment from the other atypical B
344 cell subsets, while cluster 3 and cluster 5 atypical B cells are more strongly connected, in line
345 with the results of the trajectory analysis. Collectively, these results point to different
346 developmental pathways for atypical B cells that are connected to different functional roles in
347 the immune response.

348

349 **All three atypical B cell subsets are found in malaria-experienced children and adults**
350 **irrespective of parasite exposure levels**

351 The identification of atypical B cell clusters by transcriptomics analysis was based on four
352 samples from two children. To validate our findings in a larger number of malaria-susceptible
353 children and extend our analysis to malaria-protected adults, we turned to an analysis of these
354 cells by flow cytometry. In the single-cell transcriptomics analysis, we observed that the three
355 clusters with atypical B cells could be distinguished by differences in expression level of *ITGAX*
356 (encoding CD11c) and *CD86* (**Figure 5A**). We therefore sorted three subsets of atypical B cells
357 based on expression of CD11c and CD86 (**Figure 5B, Figure S12**) and used bulk RNA-seq
358 analysis to confirm that these subsets have similar gene expression profiles as the three
359 transcriptomics clusters identified by scRNA-seq (**Figure 5C**).

360 Using spectral flow cytometry, we next aimed to study the abundance of each atypical B cell
361 subset and their longevity in the absence of antigen stimulation and infection-driven
362 inflammation. To this end, we included samples from nine children and ten adults collected
363 following known *Plasmodium* exposure and months to years later after a period with low
364 *Plasmodium* exposure due to highly effective insecticide spaying (*41, 42*) (**Figure 5D, Table**
365 **S1**). B cells were phenotyped using a panel of 18 surface and intracellular markers that would
366 allow us to identify the three atypical B cell subsets and analyze these for the expression of
367 markers previously shown to be positively (CD19, CD20, CD11c, FcRL5, CD83, CD86, CD95,
368 CXCR3, T-bet) or negatively (CD24, CD38, CXCR5) associated with activated and atypical B
369 cells (*22*). To find the atypical B cell subsets identified in our transcriptomic analysis, we first
370 gated manually on $CD19^{+}CD20^{+}CD21^{-}CD27^{-}IgG^{+}CD11c^{+}$ atypical B cells (**Figure S13**). The
371 atypical B cells from all samples were then plotted in a composite UMAP based on the
372 expression of the 12 cell surface and intracellular markers previously shown to be associated
373 with activated and atypical B cells (**Figure S14**).

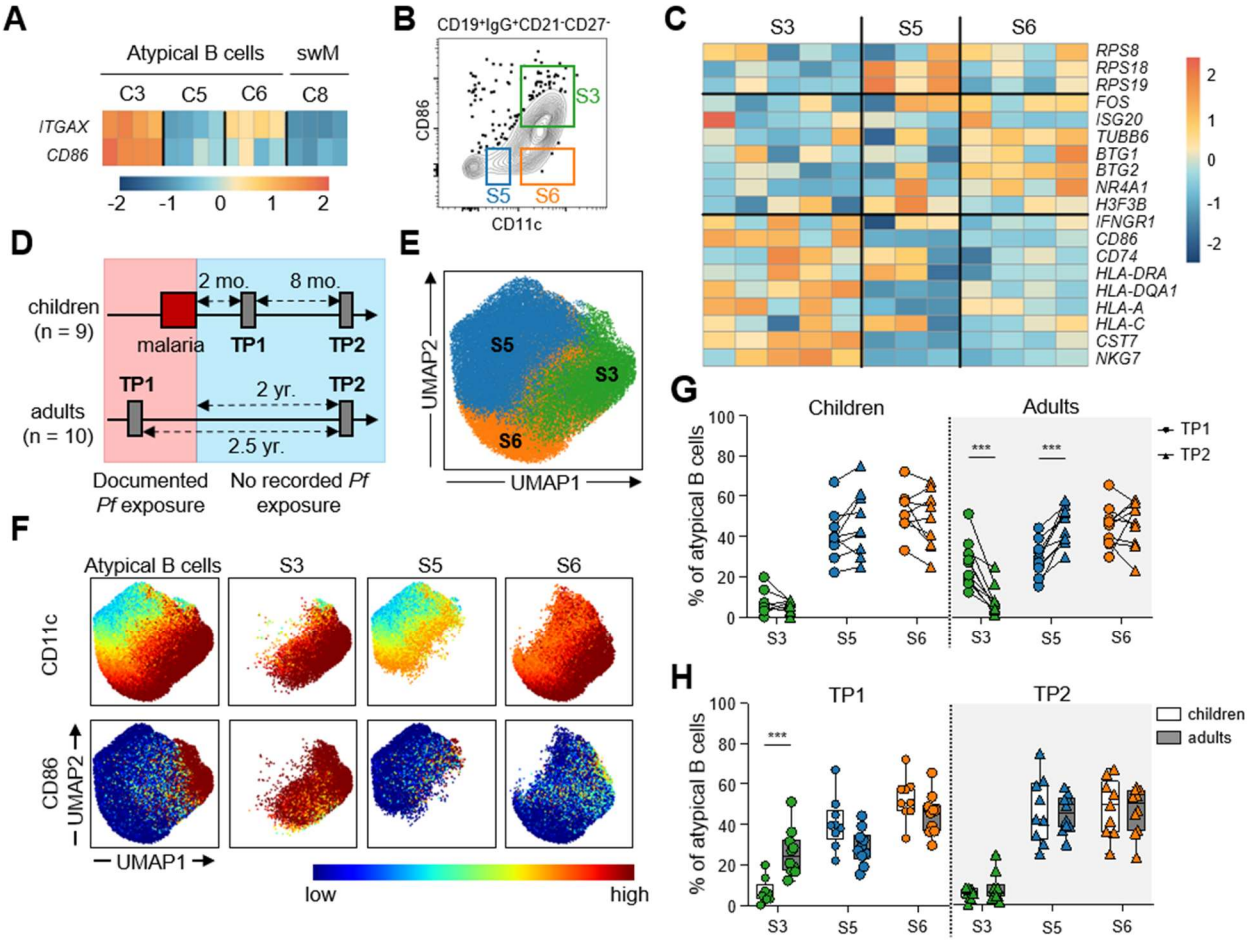

Figure 5: Dynamics of atypical B cell subsets in children and adults. A) Gene expression profiles of differentially expressed genes encoding cell surface proteins CD11c and CD86 in atypical B cell clusters 3, 5, and 6, as well as resting switched memory B cells (swM, cluster 8), used to distinguish atypical B cell subsets by flow cytometry. **B)** Gating strategy to sort atypical B cell subsets based on CD11c and CD86 expression. **C)** Expression of genes that underlie the different functional profiles of the three atypical B cell clusters (compare with Figure 3D) in flow-sorted atypical B cells subsets. **D)** Schematic overview of sample collection for children and adults during known *P. falciparum* (*Pf*) exposure and in the absence of exposure to *P. falciparum*. **E)** Composite UMAP projection of atypical B cells from all 38 samples. Subsets were defined based on expression of CD11c and CD86 and were named according to the corresponding clusters defined by single-cell RNA-sequencing analysis. **F)** CD11c and CD86 expression projected onto the UMAP of all atypical B cells as well as each of the three subsets individually. **G)** Relative size of each atypical B cell subset in children (n = 9) and adults (n = 10) at the first time point (TP1; circles) and second time point (TP2; triangles). **H)** Comparison of relative subset sizes between children and adults at each time point. Statistical analysis was performed using a Wilcoxon matched-pairs signed rank test for paired data (E) or a Mann-Whitney test for unpaired data (F) with a 10% false discovery rate using the two-stage step-up method of Benjamini, Krieger, and Yekutieli. * P < 0.05; ** P < 0.01; *** P < 0.001.

395 Next, we used the unsupervised clustering tool FlowSOM to identify three distinct atypical B cell
396 subsets based on the expression of CD11c and CD86 (**Figure 5E**). Projection of these subsets
397 onto the UMAP showed that the expression of *ITGAX* and *CD86* matched the cell surface
398 expression signatures of subset 3 ($CD11c^{hi}CD86^{+}$), subset 5 ($CD11c^{int}CD86^{-}$), and subset 6
399 ($CD11c^{hi}CD86^{-}$), (**Figure 5F**). We will refer to these subsets with the number corresponding to
400 the matching transcriptomics cluster, i.e., flow cytometry subset 3 for cells matching
401 transcriptomics cluster 3. We then determined the relative abundance of these three subsets
402 among all atypical B cells. In children, most atypical B cells belonged to subset 6 (~50%) and
403 subset 5 (~40%). The relative abundance of the subsets did not change between time points
404 (**Figure 5G**, **Figure S15**). This could be the result of the timing of sample collection. At two
405 months post-malaria in a low transmission setting, transient changes to the atypical B cell
406 population induced by malaria may have already reverted to baseline. In adults, the first sample
407 was collected during a period of high *Plasmodium* exposure. Interestingly, the proportion of
408 subset 3 atypical B cells was larger in adults than in children at the first time point but decreased
409 to the level seen in children after a period of minimal parasite exposure (**Figure 5H**). This was
410 also true when expressing the abundance of subset 3 atypical B cells as a percentage of total B
411 cells (**Figure S15**). Simultaneously, we observed an increase in the relative proportion of subset
412 5 among all atypical B cells between the two time points in the adults, although the percentage
413 of subset 5 atypical B cells among total B cells did not change (**Figure 5G**, **Figure S15**).
414 Collectively, these results demonstrate that we were able to distinguish three subsets of atypical
415 B cells by flow cytometry and that the composition of the atypical B cell population changes in
416 relation to parasite exposure.

417

418 **Atypical B cells express higher levels of CXCR3 and CD95 in adults as compared to**
419 **children**

420 To map additional differences in the phenotype between the three subsets of atypical B cells,
421 we plotted the mean fluorescence intensity of CD21, CD27, and the 12 markers that were
422 previously observed to be positively or negatively associated with activated or atypical B cells
423 for all three subsets as well as IgG^+ resting memory B cells ($CD21^-CD27^-$). We observed that
424 subset 3 had the most 'atypical' surface marker expression pattern, with the highest expression
425 of CD19, CD20, CD11c, FcRL5, CD95, and T-bet (**Figure 6A**, **Figure S16**).

426 We were also interested in potential differences in phenotype between atypical B cells from
427 malaria-experienced children and adults. At the second time point, after months to years of no
428 chronic immune activation, the distribution of atypical B cell subsets was similar between
429 children and adults (**Figure 5H**). However, we noticed that their atypical B cells had a distinct
430 localization when projected onto the UMAP (**Figure 6B**). This observation suggests that atypical
431 B cells from children and adults differ in the expression of one or more other markers.
432 Overlaying the expression of other markers in our flow cytometry panel onto the UMAP revealed
433 that atypical B cells in adults extended into the UMAP area where cells expressed high levels of
434 CXCR3 and CD95 (**Figure 6C, D**). To quantify this, we analyzed the percentage of $CXCR3^+$ and
435 $CD95^+$ cells in each subset. Adults showed more $CXCR3^+$ cells in all atypical B cell subsets as
436 compared to children (**Figure 6E**), and more $CD95^+$ cells in subsets 5 and 6 (**Figure 6F**).
437 Collectively, this difference in CXCR3 and CD95 expression between children and adults points
438 towards additional heterogeneity among atypical B cells that may be connected to differences in
439 immune status or parasite exposure levels.

440

441 **All subsets of atypical B cells harbor *P. falciparum*-specific cells**

442 To determine whether the different atypical B cell subsets develop in response to antigen during
443 infection or through bystander activation, we used antigen tetramers to detect B cells with

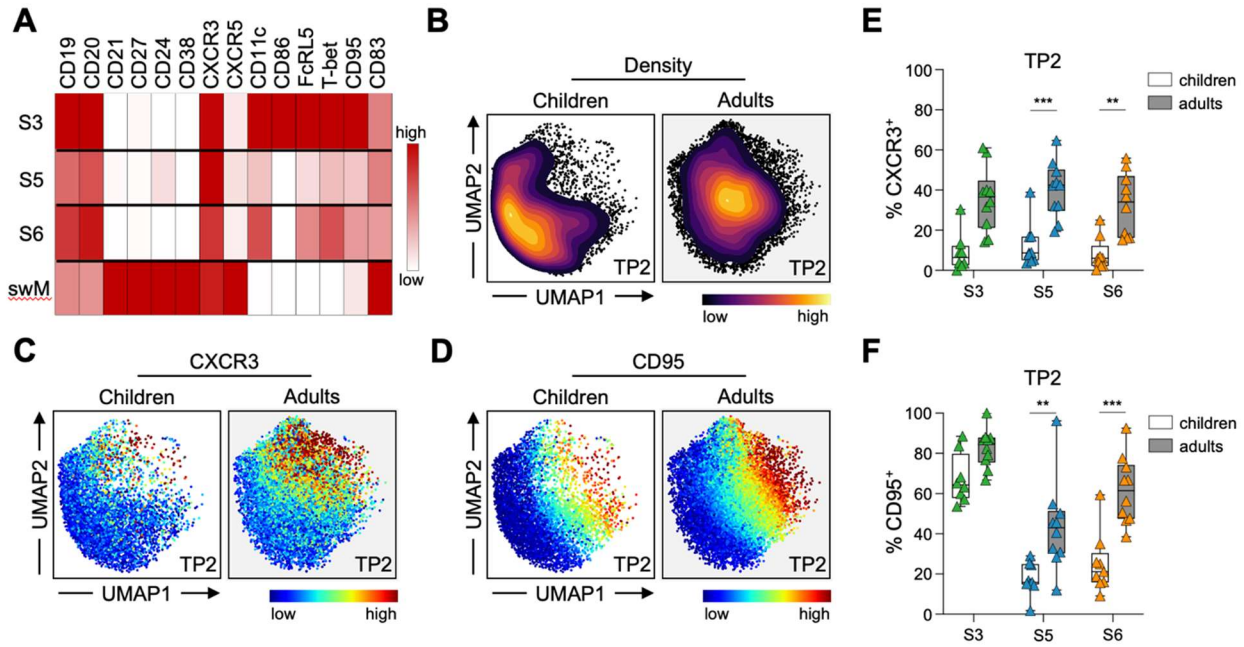

Figure 6: Expression of T-bet and CXCR3 in atypical B cell subsets. A) Relative median fluorescence intesity of 14 surface and intracellular markers in subsets (S) 3, 5, and 6 and in resting switched memory B cells (swM). **B)** Density UMAP plots of atypical B cells detected at the second time point in children and adults. **C-D)** Projection of CXCR3 (C) and CD95 (D) expression in atypical B cells at the second time point projected onto the UMAPs for children and adults. **E-F)** Percentage of $CXCR3^+$ (E) and $CD95^+$ (F) cells within atypical B cell subsets. For each subset, only individuals with >50 cells at both time points were included in the analysis. Statistical analysis was performed using a Mann-Whitney test with a 10% false discovery rate using the two-stage step-up method of Benjamini, Krieger, and Yekutieli. * $P < 0.05$; ** $P < 0.01$; *** $P < 0.001$.

456 specificity to two *P. falciparum* proteins: merozoite surface protein 1 (MSP1) and apical
457 membrane antigen 1 (AMA1). Both antigens are known to elicit strong IgG responses in children
458 and adults (*43*). Since both MSP1 and AMA1 tetramers were labeled with the same
459 fluorochromes, MSP1-specific and AMA1-specific B cells are together referred to as
460 MSP1/AMA1-specific (**Figure S13**). First, we overlayed the MSP1/AMA1-specific B cells onto
461 the previously generated UMAPs of subset 3, 5, and 6 atypical B cells. Antigen-specific cells
462 were identified in all subsets (**Figure 7A**). We then quantified the number of antigen-specific
463 cells in each of the three atypical B cell subsets and observed that the distribution of
464 MSP1/AMA1 B cells over the three subsets mirrored their total size (**Figure 7B**). Finally, we
465 analyzed CXCR3 and CD95 expression among MSP1/AMA1-specific atypical B cells in adults.
466 Approximately 25 - 40% of all MSP1/AMA1-specific atypical B cells were CXCR3^{+}, with no clear
467 pattern related to subset identity (**Figure 7C**). In contrast, nearly all MPS1/AMA1-specific
468 atypical B cells in all three subsets expressed CD95, which was an increase as compared to all
469 atypical B cells in subsets 5 and 6 (**Figure 7D**). Increased CD95 expression was also observed
470 in Spike-specific B cells in recovered COVID-19 patients (*44*) and suggests that these cells
471 recently underwent antigen-driven activation. Collectively, these results suggest that all three
472 subsets of atypical B cells develop in response to antigen stimulation.

473

474 **Differences in the level of antibody secretion in atypical B cell subsets receiving T cell**
475 **help**

476 Recently, Hopp et al. observed that bulk atypical B cells express higher levels of markers
477 associated with T cell interactions than memory B cells (*17*). With the help of activated T
478 follicular helper cells, atypical B cells could be stimulated to secrete antibodies, although
479 antibody concentrations were much lower than for memory B cells (*17*). Based on our

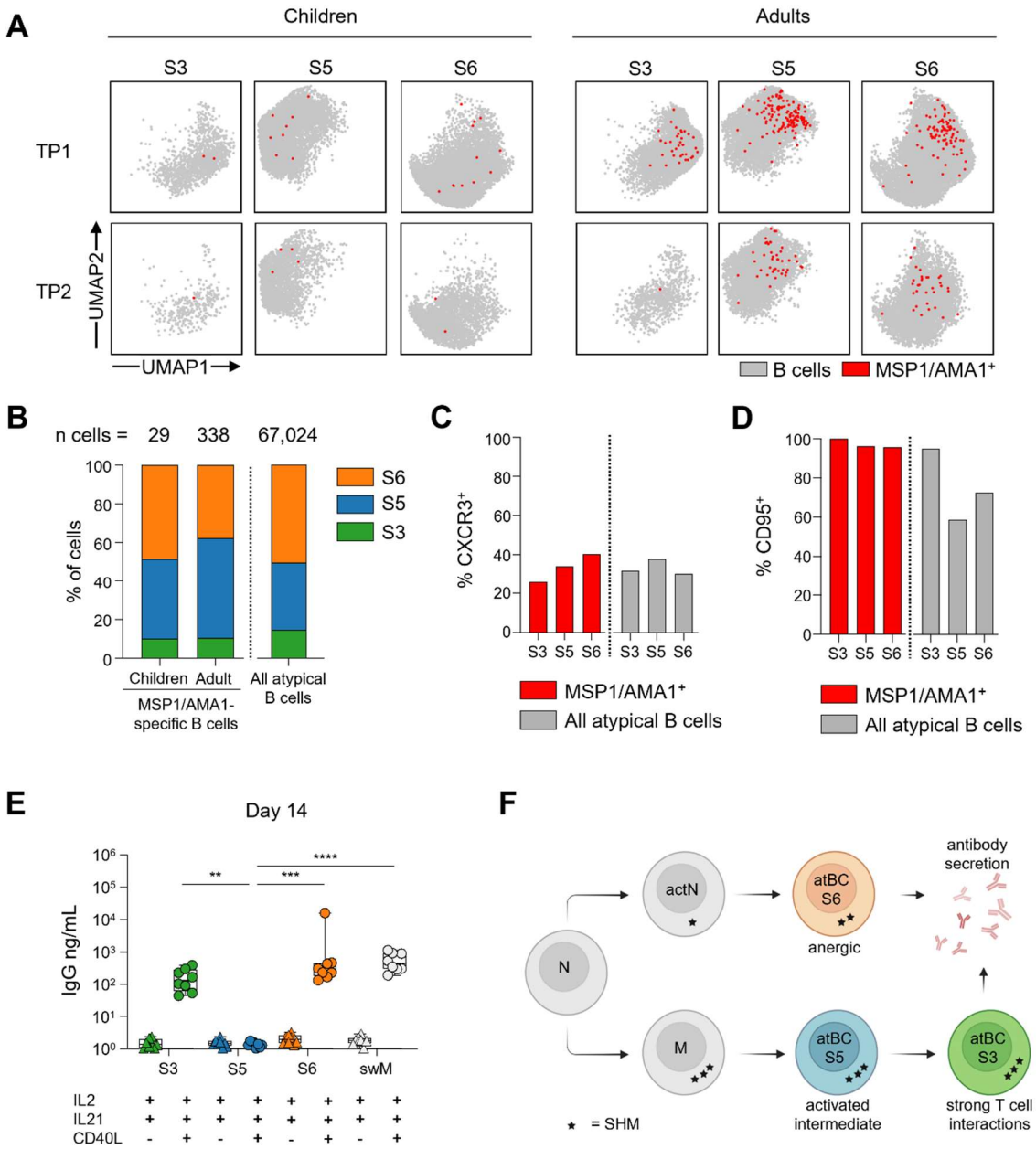

Figure 7: Antigen-specificity and antibody secretion among the three atypical B cell subsets. A) Projection of MSP1/AMA1-specific B cells (red) onto the UMAPs of atypical B cell subsets, shown separately for time point 1 (TP1) and time point 2 (TP2) in 9 children and 10 adults. **B)** Distribution of all MSP1/AMA1-specific B cells over the three atypical B cell subsets in children and adults. Data from both time points were combined. **C)** Percentage of all CXCR3$^+$ antigen-specific cells in each atypical B cell subset for adult samples. **D)** Percentage of all CD95$^+$ antigen-specific cells in each atypical B cell subset for adult samples. **E)** IgG concentration in culture supernatant after 14 days of in vitro culture. A one-way ANOVA was used to test for statistically significant differences between the groups. P values shown are from Kruskal-Wallis post hoc test. ** $P < 0.01$; *** $P < 0.001$; **** $P < 0.0001$. **F)** Proposed model of the effector functions and developmental pathways of atypical B cell subsets.

492 observations that only two out of the three atypical B cell subsets expressed markers involved in
493 T cell interactions (S3 and S6), we sought to determine which atypical B cell subsets can be
494 induced to secrete antibody under T-cell dependent activation. To this end, we FACS-sorted the
495 three atypical B cell subset based on CD11c and CD86 expression, as well as switched memory
496 B cells from eight malaria-experienced adults (**Figure S12**). We then cultured each B cell
497 population with CD40L-expressing 3T3 cells supplemented with IL-2 and IL-21 to mimic T-cell
498 dependent stimulation, and measured IgG production after 7 and 14 days. The same culture
499 conditions without CD40L-expressing 3T3 cells were included as a negative control. The
500 distribution of atypical B cells over the three subsets was reflective of high *P. falciparum*
501 exposure, allowing us to interrogate their function in terms of recent antigen exposure (**Figure**
502 **S17A**). We found that both subset 3 and subset 6 secreted IgG in the presence of T-cell help.
503 On day 7, the IgG concentration was lower than that produced by switched memory B cells
504 (**Figure S17B**), but this difference disappeared by day 14 (**Figure 7E**). Subset 5 atypical B cells
505 secreted only minimal amounts of IgG under these conditions. These results suggest that most
506 but not all atypical B cells can differentiate into antibody-secreting cells upon T-cell dependent
507 activation.

508

509 **DISCUSSION**

510 Atypical B cells accumulate in a range of conditions that share chronic immune activation as the
511 common denominator, including chronic or repetitive infection and autoimmunity. Attempts to
512 understand the function of these cells have resulted in conflicting observations. We
513 hypothesized that these different observations are caused by heterogeneity among atypical B
514 cells and that the underlying subsets are indistinguishable with the markers conventionally used
515 to define atypical B cells. Here, we used multimodal single-cell measurements to better define

516 the heterogeneity among atypical B cells using samples from individuals with chronic
517 *Plasmodium* exposure. We identified novel subsets of atypical B cells, each with a unique
518 transcriptional program and cell surface marker signature, that are associated with different
519 effector functions in the host immune response. Using spectral flow cytometry, we confirmed the
520 presence of these atypical B cell subsets in a cohort of malaria-experienced children and adults,
521 determined that they can develop in response to antigen stimulation, and assessed their ability
522 to differentiate into antibody-secreting cells.

523

524 We generated single-cell sequencing data for almost 21,500 B cells, of which we were able to
525 assign slightly more than 14,000 cells to one of 10 phenotypically defined B cell populations.
526 Among these were just over 4,000 cells that belonged to three clusters containing
527 phenotypically defined atypical B cells. Two other recent studies have attempted to assess
528 potential heterogeneity among atypical B cells using single-cell transcriptomics approaches.
529 Holla *et al*. subclustered 199 B cells from malaria-experienced individuals with an atypical
530 transcriptomics profile and observed three subsets that were mainly discriminated by isotype
531 usage (i.e., IgD^+IgM^+, IgD^+IgM^{lo}, and IgD^-IgG^+ atypical B cells) (*11*). Too few cells were present
532 in that data set to observe subclusters within the IgD^-IgG^+ atypical B cell group, which was the
533 focus of our study. Sutton *et al.* analyzed a larger number of IgD^- B cells (7,167 cells from
534 malaria-experienced individuals and 5,813 cells from individuals not exposed to *Plasmodium*
535 infection) that were divided into three atypical B cell clusters and several other B cell clusters
536 (*3*). However, reanalysis of this data set did not reveal a clear separation into the same subsets
537 of atypical B cells that we observed in our data set. The main reason for this observation could
538 be that Sutton *et al.* used samples from immune adults who had not recently experienced a
539 malaria episode. Likewise, the gene expression profiles of atypical B cell subsets 3 and 6 from
540 malaria-experienced adults that were generated in this study were very similar (**Figure S18**),

541 although differences in expression of genes that underlie the different function profiles of the
542 three atypical B cells subsets were still apparent (**Figure S5C**). A malaria episode may drive
543 these functionally distinct gene expression programs, followed by their convergence in the
544 absence of such a strong stimulus.

545

546 Using our single-cell transcriptomics data set of atypical B cells, we confirmed similarities in
547 gene expression between our three atypical B cell clusters and bulk RNA sequencing
548 transcriptional programs that have previously been reported for atypical B cells (*10, 12*).
549 However, we also discovered that some genes previously linked to atypical B cells were
550 expressed in only one of these three clusters and may be connected to the different functional
551 profiles of these cells. For example, CD72 negatively regulates B cell activation (*27*). *CD72* was
552 uniquely expressed in cluster 6 that has a profile of senescence or anergy. Cluster 3, on the
553 other hand, expressed higher levels of the gene encoding CD68, a transmembrane glycoprotein
554 that is mainly associated with the endosomal/lysosomal compartment in monocytes and
555 macrophages, but is also expressed by lymphocytes (*45, 46*). This observation may be related
556 to the pathways of antigen processing and exocytosis that were upregulated in this cluster.

557

558 Using differentially expressed surface markers, we were able to identify three corresponding
559 subsets of atypical B cells by flow cytometry. All three subsets harbored *P. falciparum*-specific B
560 cells, suggesting that each of these subsets can develop as part of a specific response to
561 pathogen-derived antigens and not merely through bystander activation. The lower levels of
562 somatic hypermutation set cluster 6 apart from clusters 3 and 5. Indeed, RNA velocity and B cell
563 receptor repertoire analyses suggested that cluster 6 formed a compartment that was mostly
564 separated from clusters 3 and 5, and followed a different developmental trajectory. The RNA
565 velocity analysis, the increase in percentage of B cell clones that were shared between clusters

566 3 and 5 over time as the B cell response contracted to baseline levels, and the observation that
567 the decrease in subset 3 atypical B cells over time was paralleled by a relative increase in the
568 size of subset 5 together suggest that atypical B cells in subsets 3 and 5 are developmentally
569 related.

570

571 Based on these data, we propose the following working model (**Figure 7F**). Chronic immune
572 activation results in the development of three subsets of atypical B cells. Subset 6 is derived
573 from activated naïve B cells and has relatively low levels of somatic hypermutation. These
574 characteristics are similar to atypical B cells in SLE patients that arise through extrafollicular
575 activation. Under conditions that mimic the interaction with $CD4^+$ T cells, subset 6 atypical B
576 cells can further differentiate into short-lived antibody-secreting cells, although these cells are
577 likely to have a high activation threshold. The main developmental trajectory of subset 3 atypical
578 B cells is from memory B cells via an activated subset 5 state. These cells have undergone high
579 levels of somatic hypermutation, consistent with the normal development of memory B cells.
580 Subset 3 atypical B cells are primed for interactions with T cells and will differentiate into
581 antibody-secreting cells upon stimulation by T cells (*47*). Additionally, these cells express
582 proteins that may modulate the function of T cells in return. Subset 5 atypical B cells express
583 lower levels of markers typically associated with atypical B cells, such as FcRL5, T-bet and
584 CD11c, and do not differentiate into by interaction with T cells alone. Other stimuli, such as BCR
585 engagement, additional cytokines, or TLR engagement may drive the differentiation of this
586 subset into antibody-secreting cells. Indeed, Sullivan *et al*. reported that a subset of atypical B
587 cells that expressed lower levels of FcRL5 showed more antibody secretion upon BCR
588 stimulation than $FcRL5^+$ atypical B cells (*10*). Collectively, the functional profiles of the three
589 clusters of atypical B cells recapitulate many of the observations that have been made about the
590 atypical B cell population as a whole. Our results indicate that specific subsets of atypical B cells

591 are likely responsible for conflicting observations related to anergy/tolerance, immune-
592 modulation, and the ability to differentiate into antibody-secreting cells.

593

594 Comparing atypical B cells between malaria-experienced children and adults revealed additional
595 heterogeneity. Adults showed a higher percentage of CXCR3^{+} cells across all three subsets of
596 atypical B cells, which did not decrease after a two-year period of minimal *P. falciparum*
597 exposure. Hopp *et al.* reported that expression of *CXCR3* is upregulated in atypical B cells in
598 response to malaria in children (*17*). The stable expression of CXCR3 in adults suggests that
599 this marker is acquired as a result of chronic antigen exposure and may play an important role
600 in the protective immune response against malaria. Sutton *et al.* observed that *Pf*MSP1-specific
601 B cells in adults expressed higher levels of CXCR3 than the total memory B cell population,
602 although the majority of these cells did not have a CD21^{-}CD27^{-} phenotype (*48*). In this study, we
603 detected CXCR3^{+} parasite-specific cells but parasite-specific cells were not enriched for CXCR3
604 expression among atypical B cells. CXCR3 is an interferon-inducible chemokine receptor
605 specific for the chemokines CXCL9, CXCL10, and CXCL11 that are themselves also induced by
606 interferon (*49*). Its function has mainly been studied in T cells where it is required for trafficking
607 of T cells to sites of inflammation (*50*). The profile of trafficking receptor expression in atypical B
608 cells, including CXCR3, has been linked to the propensity of T-bet^{hi} B cells to take up residency
609 in the spleen and bone marrow (*51*). While no data is available for the tissue distribution of
610 atypical B cells in malaria-experienced individuals, it would make sense for parasite-specific B
611 cells to home to the spleen, since this is the main anatomical location for the removal of
612 parasite-infected erythrocytes and cellular debris from the circulation. In this regard, it is
613 interesting to note that the elevated expression of T-bet and CD74 in subset 3 atypical B cells
614 fits the profile of memory B cells that reside in the spleen (*51, 52*), indicating that the loss of
615 these cells in the circulation could be the result of migration into the spleen. However, the

616 observation that the percentage of CXCR3^{+} atypical B cells does not change over time with
617 minimal parasite exposure suggests that the expression of this marker by itself does not direct
618 homing of B cells to tissues. This notion is strengthened by the recent finding that CXCR3
619 ablation in murine B cells has no effect on the establishment and maintenance of lung-resident
620 memory B cells (*53*). Instead, CXCR3 should probably be considered a marker of activation or
621 prior activation.

622

623 One of the complications of studying atypical B cells is that different markers have been used to
624 define atypical B cells. In this study, our definition of atypical B cells is based on how these cells
625 are typically identified in the HIV and malaria fields (CD21^{-}CD27^{-}) and information from a recent
626 single-cell RNA sequencing study that reported CD11c as the most informative cell surface
627 marker for the identification of atypical B cell lineages (*3*). Our definition of atypical B cells as
628 IgG^{+}CD21^{-}CD27^{-}CD11c^{+} also fits the definition of DN2 B cells, which is how these cells are
629 commonly referred to in the autoimmunity field (IgD^{-}CD27^{-}CD21^{-} CD11c^{+}) and follows recently
630 published recommendations for how these cells should be defined (*22*). Not all of the cells that
631 fall within our definition of atypical B cells are T-bet^{+}, which may complicate translating our
632 findings to studies that use T-bet (with or without CD11c) as a defining marker for atypical B
633 cells (*48, 54, 55*).

634

635 In conclusion, we found that atypical B cells can be divided into at least three functionally
636 distinct subsets. These findings reconcile many of the conflicting observations that have been
637 made about atypical B cells and provide insight into their function in the immune response
638 against infection. Our study also highlights that the composition of the atypical B cell population
639 can alter with changes in pathogen exposure levels. The selection of individuals and timing of
640 sample collection therefore warrants careful consideration when analyzing atypical B cells and

641 their functional profile. Although the transcriptomes of atypical B cells in chronic infections and
642 autoimmunity are remarkably similar (*11*), our observations about atypical B cells in malaria-
643 experienced individuals will need to be confirmed in other disease models. Collectively, our
644 results suggest that a large fraction of atypical B cells may contribute to a productive and
645 antigen-specific immune response against infection.

646

647 **MATERIALS AND METHODS**

648 **Study design and ethics approval**

649 The objective of this study was to assess transcriptional and functional heterogeneity among
650 atypical B cells to determine the function of these cells in the host immune response to infection.
651 Individuals included in this study (n = 29) were residents of the Nagongera sub-county in Tororo
652 District, Uganda. This region was historically characterized by extremely high malaria
653 transmission intensity, with an estimated annual entomological inoculation rate of 125 infectious
654 bites per person per year (*56*). Since 2015, multiple rounds of insecticide spraying (IRS) have
655 dramatically reduced malaria incidence compared with pre-IRS levels (*41*). Individuals were
656 selected for inclusion into this study based on age and *P. falciparum* exposure. In addition,
657 children were selected based on the availability of samples collected at set times relative to a
658 malaria episode (**Table S1**). All individuals included in this study were enrolled in The Program
659 for Resistance, Immunology, Surveillance, and Modeling of Malaria (PRISM) program (*57*) and
660 have provided written consent for the use of their samples for research. The PRISM cohort
661 study was approved by the Makerere University School of Medicine Research and Ethics
662 Committee (SOMREC), London School of Hygiene and Tropical Medicine IRB, the University of
663 California, San Francisco Human Research Protection Program, and the Stanford University

664 School of Medicine IRB. The use of cohort samples for this study was approved by the
665 Institutional Review Board of the University of Texas Health Science Center at San Antonio.

666

667 **B cell isolations**

668 Cryopreserved PBMCs were thawed in a 37°C water bath and immediately mixed with pre-
669 warmed thawing medium (IMDM/GlutaMAX supplemented with 10% heat-inactivated FBS (USA
670 origin) and 0.01% Universal Nuclease (Thermo, cat. no. 88700). After centrifugation (250 × g, 5
671 min), the cell pellet was resuspended in thawing medium. A sample of cells was mixed 1:1 (v/v)
672 with 0.2% trypan blue solution in PBS, and viable cells were counted using a Cellometer Mini
673 (Nexcelom) automated cell counter. Next, cells were centrifuged (250 × g, 5 min) and
674 resuspended in isolation buffer (PBS supplemented with 2% heat-inactivated FBS and 1 mM
675 EDTA) at 50 million live cells/mL and filtered through a 35 µm sterile filter cap (Corning, cat. no.
676 352235) to break apart aggregated cells. B cells were isolated using the EasySep Human B Cell
677 Isolation Kit (StemCell, cat. no. 17954) or the MojoSort Human Pan B Cell Isolation Kit
678 (BioLegend, cat. no. 480082) according to the manufacturer's instructions.

679

680 **Flow cytometry staining for single-cell analysis**

681 Isolated B cells were washed with PBS (250 × g, 5 min), resuspended in 1 ml of PBS containing
682 1 µl live/dead stain (LIVE/DEAD Fixable Aqua Dead Cell Stain Kit (Thermo Fisher Scientific, cat.
683 no. L34965), and incubated for 30 min on ice. Subsequently, cells were washed with cold PBS
684 containing 1% bovine serum albumin (BSA) (250 × g, 5 min) and incubated in labeling buffer
685 (total volume of 100 µl) containing PBS, 1% BSA, 5 µl Human TruStain FcX (Biolegend, cat. no.
686 422301) and 1% dextran sulfate (Sigma-Aldrich, cat. no. 42867-5G) for 10 min at 4°C before

687 incubating a further 30 min at 4°C with an antibody cocktail to label B cell surface markers
688 (**Table S7**). Before acquisition on a BD FACS AriaII cell sorter, cells were washed with cold PBS
689 containing 1% BSA, centrifuged (250 × g, 5 min, 4ºC), diluted to 20-30 million cells/mL in cold
690 PBS containing 1% BSA, and filtered into a FACS tube through a 35 µm sterile filter cap
691 (Corning, cat. no. 352235) to break apart aggregated cells. Lymphocytes were gated using
692 forward and sideward scatter, followed by doublet exclusion. Cells were then gated on live cells,
693 followed by $CD19^{+}CD10^{-}CD20^{+}$ B cells. Naive B cells ($CD21^{+}CD27^{-}$) and antigen-experienced B
694 cells (all other B cells) were separated based on CD21 and CD27 expression and sorted into
695 cold PBS containing 1% BSA. An average of 37,000 antigen-experienced B cells were mixed
696 with naïve B cells up to a total of 50,000 B cells (**Table S2**). This resulted in an enrichment of
697 antigen-experienced cells from an average of 49% in the original B cell pool to an average of
698 74% in the final cell suspension. Cells were immediately processed for single-cell sequencing.

699

700 **Single-cell gene expression, V(D)J, and feature barcoding library preparation**

701 B cells were counted with a hemocytometer and run on a Chromium 10x controller (10x
702 Genomics) in individual lanes with a targeted recovery rate of 10,000 cells per lane, according
703 to the manufacturer's instructions. Library preparation was completed following the
704 recommended protocols for Chromium Single Cell 5' Gene Expression kit as well as 5' Feature
705 Barcode and V(D)J Enrichment kits (**Table S8**). Libraries were sequenced using the Illumina
706 NovaSeq6000 (paired-end 150 bp) and HiSeq (paired-end 100 bp) platforms.

707

708 **Single-cell RNA-seq data analysis**

709 Sequencing reads were mapped to the human reference genome (hg38) and assigned to
710 individual cells of origin using cell-specific barcodes in Cell Ranger (10x Genomics) version
711 3.1.0. The sequencing data were then processed using Seurat version 3.2.3, following their
712 default pipeline as follows. Low-quality cells with high (>2500) or low (<200) UMI counts were
713 filtered from the samples. In addition, to prevent antibody isotype or V(D)J-gene segment usage
714 from influencing the clustering of cells, we removed all IGH, IGK and IGL transcripts from the
715 single cell data before clustering and UMAP visualization, as proposed by Steward *et al*. (*20*).
716 Gene expression levels for each cell were normalized by total expression, multiplied by a scale
717 factor (10,000), and log-transformed. Cells with > 5% mitochondrial reads were excluded
718 because these are likely damaged or dying cells that have lost much of their cytoplasmic
719 mRNA. Gene expression values for all genes in all clusters are provided in **Table S9**. We
720 determined the top 2000 most variable genes based on their average expression and
721 dispersion. Principal component analysis was performed on highly variable genes to reduce the
722 dimensionality of the data. We performed clustering using the Louvain algorithm implemented in
723 the *FindClusters* function of Seurat (algorithm = 1, resolution = 0.5, dims. use = 1:20) and
724 displayed the clusters using UMAP. One outlier cluster consisting of 13 cells that were most
725 likely T cells was removed from further analysis. Because cells from all samples were
726 distributed evenly across the UMAP (**Figure S3**), no batch corrections were performed. We
727 identified the cluster-specific marker genes conserved across different samples using the
728 *FindConservedMarkers* function (default parameters) from Seurat. To identify differentially
729 expressed genes between a pair of clusters, we used the *FindMarkers* function from Seurat
730 (with parameters *min.pct* = 0.20, and log2FC = 0.25), and additionally filtered genes using a
731 false discovery rate of 0.05. Violin plots, dot plots, and UMAP plots overlaid with gene
732 expression level were generated using standard Seurat functions. Reactome pathway analysis
733 was performed using differentially expressed genes that were upregulated in pairwise cluster
734 comparisons. The top 3 - 5 pathways with FDR-adjusted P value < 0.01 were selected for visual

735 representation in **Figure 3C**. The full set of Reactome analysis results and differentially
736 expressed gene lists are provided in **Tables S5** and **S6**. For heatmaps in Figures 3, gene
737 expression values for the four samples were first divided by the average value for all clusters for
738 that donor to account for donor-to-donor variation. The data points were then z-scored across all
739 clusters and samples prior to plotting heatmaps using the color palette 'Hiroshige' from the R
740 package MetBrewer.

741

742 **Single-cell RNA-sequencing gene signature score analysis**

743 We performed gene signature score analysis as described in (*11*). Briefly, gene expression data
744 from the Seurat object were scaled (z-score across each gene) to remove bias towards highly
745 expressed genes. A cell-specific signature score was computed by first sorting the normalized
746 scaled gene expression values for each cell followed by summing up the indices (ranks) of the
747 signature genes. These signature scores were then projected onto the transcriptomics-based
748 UMAP.

749

750 **Single-cell surface marker analysis**

751 From the single-cell RNA sequencing Seurat object, we extracted the antibody capture
752 component (assay = ADT), normalized the antibody matrix using CLR normalization (Seurat
753 method *NormalizeData*), and then scaled the antibody matrix using Seurat routine *ScaleData*.
754 This normalized and scaled antibody matrix was then used to define the following populations of
755 B cells by phenotype: 1) DN1 B cells: $CD27^{-}IgG^{+}CD21^{+}CD11c^{-}$, 2) DN2 B cells: $CD27^{-}$
756 $IgG^{+}CD21^{-}CD11c^{+}$, 3) DN3 B cells: $CD27^{-}IgG^{+}CD21^{-}CD11c^{-}$, 4) DN4 B cells: $CD27^{-}$
757 $IgG^{+}CD21^{+}CD11c^{+}$, 5) Resting naïve B cells: $CD27^{-}IgM^{+}CD21^{+}$, 6) Activated naïve B cells:

758 $CD27^-IgM^+CD21^-$, 7) Resting switched memory B cells: $CD27^+IgG^+CD21^+$, 8) Activated switched
759 memory B cells: $CD27^+IgG^+CD21^-$, 9) Resting unswitched memory B cells: $CD27^+IgM^+CD21^+$,
760 and 10) Activated unswitched memory B cells: $CD27^+IgM^+CD21^-$. The UMAP plots highlighting
761 corresponding cell categories were generated using Seurat. Distributions of cell surface
762 expression of the markers CD21 and CD27 (**Figure S4**), as well as CD11c and CXCR3 (**Figure**
763 **S6**) for individual clusters were plotted using the above mentioned normalized and scaled
764 antibody matrix, and employing the 2D kernel density function *kde2d* from the R package
765 *MASS*.

766

767 **Single-cell B cell receptor analysis**

768 Single-cell B cell receptor sequencing data was first processed using the command *changeo-*
769 *10x*. Single-cell heavy chain variable region sequences were then analyzed using the
770 Immcantation pipeline. First, the Immcantation package Change-O (v0.4.4) was used to align
771 lymphocyte receptor sequences to germline sequences for downstream analyses (*58*). Isotype-
772 specific data files were converted into standardized tab-delimited database files required for
773 subsequent Change-O modules to operate using IgBLAST (v1.14.0), which is included in
774 Change-O. The frequency of somatic hypermutations was calculated as described previously
775 (*23*). Average frequencies for each donor and cluster are reported.

776 To calculate the percentage of clonal expansion within clusters or clonal connections between
777 clusters, genotyping was performed using the routine *tigger-genotype*, followed by analysis of
778 clonally related B cell receptor sequences using a custom Perl script available for download at
779 https://github.com/embunnik/clonal_scores, as described in detail elsewhere (*38*).

780

781 **RNA velocity analysis**

782 RNA-velocity analysis was performed by scVelo (*59*), using the scRNA-seq data. First, gene
783 expression matrices from cell ranger were converted to scVelo compatible loom format using the
784 tool Velocyto (*60*). We exported the cluster information and the UMAP coordinates from the
785 Seurat object in .h5ad format, instead of re-computing them in scVelo. RNA-velocity analysis was
786 then performed by the scVelo routine *tl.velocity()* using its default stochastic model. RNA velocity
787 and pseudo-time plots were generated by the default scVelo routines.

788

789 **Atypical B cell sorting**

790 B cells were isolated by negative selection as described above, washed with PBS (250 × g, 5
791 min), and resuspended in 1 ml of PBS containing 1 µl live/dead stain (LIVE/DEAD Fixable Aqua
792 Dead Cell Stain Kit (Thermo Fisher Scientific, cat. no. L34965) and incubated for 30 min on ice.
793 Cells were subsequently washed with cold PBS containing 1% BSA (250 × g, 5 min, 4ºC) and
794 incubated at 4°C for 30 min with a B cell surface marker antibody cocktail (**Table S12**), added
795 up to a total volume of 100 µl with PBS containing 1% BSA. Cells were then washed with cold
796 PBS containing 1% BSA, centrifuged (250 × g, 5 min, 4ºC), diluted to 20-30 million cells/mL in
797 cold PBS containing 1% BSA, and filtered into a FACS tube through a 35 µm sterile filter cap
798 (Corning, cat. no. 352235) to break apart aggregated cells. Using a BD FACS Aria Fusion cell
799 sorter, atypical B cell subsets and switched memory cells were sorted into 1.5 mL Eppendorf
800 tubes containing IMDM/GlutaMAX supplemented with 10% heat-inactivated FBS (USA origin).
801 Cells were immediately frozen for RNA-seq or plated for in vitro B cell activation experiments.

802

803 **Bulk RNA-Sequencing**

804 RNA-seq libraries were generated following the NEBNext Single Cell/Low Input RNA Library
805 Prep Kit for Illumina (NEB #E6420S) protocol for cells, except that all DNA cleanup steps we
806 done using SparQ magnetic beads (Quantabio). In brief, 200 cells of each B cell subset were
807 FACS sorted directly into 1× NEBNext Cell Lysis Buffer in 1.7 ml low binding tubes (Corning
808 #3207). Cells were then flash frozen in liquid nitrogen for future use. For all samples, cDNA was
809 synthesized and amplified using 21 cycles. cDNA quantity and quality were assessed by
810 Invitrogen Qubit and Agilent 2100 Bioanalyzer. PCR enrichment of adaptor-ligated DNA was
811 performed using NEBext Multiplex Oligos for Ilumina (NEB #E7335S and #E7500S) following
812 the recommended number of amplification cycles based on the amount of cDNA input used in
813 the fragmentation/end prep reaction. Library quantity and quality were assessed by Invitrogen
814 Qubit and Agilent 2100 Bioanalyzer. Eighteen libraries were multiplexed and sequenced on a
815 NovaSeq600 SP 50PE flow cell. Six libraries were retrospectively removed from data analysis
816 due to low input cDNA and resulting low gene expression quality. The list of genes that were
817 differentially expressed between the three atypical B cell clusters in the scRNA-seq data set and
818 were representative of functional differences between these clusters was filtered for an average
819 expression level of 100 transcripts per million (tpm) among the remaining samples. Expression
820 values were z-scored across all samples and plotted in a heatmap.

821

822 **Staining for spectral flow analysis**

823 C-terminally biotinylated full-length *P. falciparum* 3D7 MSP1 and AMA1 were produced as
824 described previously (*43*). Antigen tetramers were synthesized by incubating protein with
825 fluorophore-conjugated streptavidin overnight at 4˚C at a molar ratio of 6:1 with rotation (**Table**
826 **S10**). B cells were isolated by negative selection as described above, washed with PBS,
827 centrifuged (250 × g, 5 min), resuspended in 1 ml of PBS containing 1 µl live/dead stain
828 (Zombie UV Fixable Viability kit (Biolegend, cat. no. 423107)) and incubated on ice for 30 min.

829 Cells were subsequently washed with cold PBS containing 1% BSA (250 × g, 5 min, 4ºC),
830 resuspended with a cocktail of 25 μM of each antigen tetramer diluted in PBS containing 1%
831 BSA to a volume of 100 μl, and incubated at 4°C for 30 min. Next, the cells were washed twice
832 with cold PBS containing 1% BSA (250 × g, 5 min, 4ºC) and incubated at 4°C for 30 min with a
833 B cell surface marker antibody cocktail (**Table S11**) with 10 μl Brilliant Stain Buffer Plus (BD,
834 cat. No. 566385) diluted in PBS containing 1% BSA up to a volume of 100 μl. The cells were
835 then washed with cold PBS containing 1% BSA (250 × g, 5 min, 4ºC), resuspended in 1 ml of
836 Transcription Factor Fix/Perm Concentrate (Tonbo, part of cat. no. TNB-0607-KIT), diluted with
837 3 parts Transcription Factor Fix/Perm Diluent (Tonbo), and incubated at 4°C for 1 hour. After the
838 incubation, the cells were washed twice with 3 ml of 1× Flow Cytometry Perm Buffer (Tonbo)
839 (300 × g, 8 min, 4ºC) and resuspended in 1× Flow Cytometry Perm Buffer with an intracellular
840 marker antibody (**Table S11**). After an incubation at 4°C for 30 min, the cells were washed twice
841 with 3 ml cold 1× Flow Cytometry Perm Buffer (300 × g, 8 min, 4ºC) and once with 3 ml cold
842 PBS containing 1% BSA, resuspended in cold PBS containing 1% BSA to 20 – 30 million
843 cells/ml and filtered into a FACS tube through a 35 μm sterile filter cap. Cells were analyzed by
844 flow cytometry immediately following intracellular staining.
845
846 **Spectral flow cytometry analysis**

847 B cells were analyzed on a Cytek Aurora spectral flow cytometer equipped with five lasers.
848 SpectroFlo QC Beads (Cytek, cat. no. SKU N7-97355) were run prior to each experiment for
849 performance tracking. Quality control and LJ tracking reports were used to ensure machine
850 performance and that settings between different runs were comparable. Paired samples were
851 processed in the same experiment and experiments performed on separate days contained
852 technical replicates. B cells isolated from pooled PBMCs from two malaria-naïve US donors
853 were used for the compensation of the live/dead stain, for the unstained control, and for

854 technical replicates. Between runs, the expression of cell surface and intracellular markers
855 showed a high correlation between these technical replicates (Spearman r = 0.98, **Figure S19**).
856 UltraComp eBeads Plus Compensation Beads (Thermo, cat. No. 01-3333-41) were used for
857 compensation of all other fluorophores. The cytometry analysis software OMIQ (Dotmatics) was
858 used for the integration and dimension reduction analysis. In short, atypical B cells were first
859 pre-gated on single/live/CD19^{+}/CD20^{+}/CD21^{-}/CD27^{-}/CD11c^{+}/IgG^{+} cells. UMAPs were then
860 created using the expression of CD19, CD20, CD24, CD38, CD83, CD86, CD95, CXCR3,
861 CXCR5, CD11c, FcRL5, and T-bet as features with default parameters (neighbors = 15,
862 minimum distance = 0.4, metric = Euclidean, random seed = 9258) and included all 38 Ugandan
863 donor samples used in this study for initial projection. To define the three atypical B cell subsets,
864 FlowSOM (*61*) was used to identify three clusters based on CD11c, FcRL5, and CD86
865 expression using the default parameters (metric = Euclidean, random seed = 1226). For the
866 projection of antigen-specific B cells onto the UMAP, gates were manually set to identify
867 populations of interest using two-dimensional displays, which were then overlaid onto the UMAP
868 projection. Mean fluorescence intensities of cell surface and intracellular markers in select B cell
869 subsets were calculated for each sample individually in OMIQ, and then averaged across
870 samples. To visualize mean fluorescence intensities in a heatmap, the average value for each B
871 cell subset was expressed as a percentage of the highest mean fluorescence intensity among
872 all subsets.

873

874 **B cell cultures**

875 One day prior to sorting B cells, wells of a 96-well plate were each seeded with 30,000
876 adherent, CD40L-expressing 3T3 cells (kind gift from Dr. Mark Connors, NIH) in 100 µl
877 IMDM/Glutamax/ 10% FBS containing 2× MycoZap Plus-PR (Lonza #VZA-2021), 100 ng/ml

878 human IL-2 (GoldBio #1110-02-50), and 100 ng/ml human IL-21 (GoldBio #1110-21-10) to
879 promote expansion and differentiation of B cells into antibody-secreting cells. As a control, one
880 plate was prepared with 100 µl IMDM/Glutamax/ 10% FBS containing 2× MycoZap Plus-PR
881 (Lonza #VZA-2021), 100 ng/ml human IL-2 (GoldBio #1110-02-50), and 100 ng/ml human IL-21
882 (GoldBio #1110-21-10), without 3T3 cells. Plates were incubated O/N at 37°C and 8% CO_2.
883 Immediately after B cell sorting, 100 cells of each B cell subset were resuspended in 100 µl
884 IMDM/Glutamax/ 10% FBS, added to the 100 µl culture media with supplements already
885 present in the plates to a total volume of 200 µl, and incubated at 37°C and 8% CO_2. After
886 seven days, 80 µl of supernatant was removed and replenished with 100 µl IMDM/Glutamax/
887 10% FBS containing 2× MycoZap Plus-PR (Lonza #VZA-2021), 100 ng/ml human IL-2 (GoldBio
888 #1110-02-50), 100 ng/ml human IL-21 (GoldBio #1110-21-10). At day 14, the IgG concentration
889 in the supernatant was determined by enzyme-linked immunosorbent assay (ELISA).

890

891 **Enzyme-Linked Immunosorbent Assays**

892 To detect IgG, 96-well ELISA plates (Corning #3361) were coated with goat anti-human IgG
893 (Sigma #I2136) antibody at a concentration of 4 µg/ ml diluted in PBS, at a total volume of 100
894 µl per well. After a one-hour incubation at 37°C or O/N at 4°C, each well was washed once
895 using slowly running (approximately 900 ml/min.) deionized water. All subsequent washes were
896 performed this way. 150 µl blocking buffer (one-third Non-Animal Protein (NAP)- Blocker (G-
897 Biosciences #786-190P) and two-thirds PBS) was added to each well to prevent non-specific
898 binding. After one hour of incubation at 37°C, the wells were washed three times and 5 µl B cell
899 culture supernatant diluted 1:20 in dilution buffer (1% NAP Blocker in PBS; total volume 100 µl)
900 was added per well. Plates were incubated for two hours at 37°C and washed five times. Then,
901 100 µl 1:2500 diluted (1% NAP Blocker in PBS) HRP-conjugated anti-human IgG antibody

902 (BioLegend #410902) was added to each well. After incubation for one hour at 37°C and three
903 washes, HRP activity was detected using 50 µl TMB (Thermo #PI34024). Plates were incubated
904 in the dark at RT and the oxidation reaction was stopped by adding 50 µl 0.18 M H_2SO_4 (Fisher
905 #FLA300-212) per well when the negative controls (wells that received buffer when test wells
906 received culture supernatant) started to color. Absorbance was measured at 450 nm using a
907 BioTek Synergy H4 microplate reader. A human IgG (Sigma #I2511) standard curve (ten three-
908 fold serial dilutions starting at 20 µg/ml) was used to quantify samples.

909

910 **References and notes**

911 1. D. Lau, L. Y. Lan, S. F. Andrews, C. Henry, K. T. Rojas, K. E. Neu, M. Huang, Y. Huang,
912 B. DeKosky, A. E. Palm, G. C. Ippolito, G. Georgiou, P. C. Wilson, Low CD21
913 expression defines a population of recent germinal center graduates primed for plasma
914 cell differentiation. *Sci Immunol* **2**, (2017).
915 2. S. F. Andrews, M. J. Chambers, C. A. Schramm, J. Plyler, J. E. Raab, M. Kanekiyo, R.
916 A. Gillespie, A. Ransier, S. Darko, J. Hu, X. Chen, H. M. Yassine, J. C. Boyington, M. C.
917 Crank, G. L. Chen, E. Coates, J. R. Mascola, D. C. Douek, B. S. Graham, J. E.
918 Ledgerwood, A. B. McDermott, Activation Dynamics and Immunoglobulin Evolution of
919 Pre-existing and Newly Generated Human Memory B cell Responses to Influenza
920 Hemagglutinin. *Immunity* **51**, 398-410 e395 (2019).
921 3. H. J. Sutton, R. Aye, A. H. Idris, R. Vistein, E. Nduati, O. Kai, J. Mwacharo, X. Li, X.
922 Gao, T. D. Andrews, M. Koutsakos, T. H. O. Nguyen, M. Nekrasov, P. Milburn, A.
923 Eltahla, A. A. Berry, N. Kc, S. Chakravarty, B. K. L. Sim, A. K. Wheatley, S. J. Kent, S. L.
924 Hoffman, K. E. Lyke, P. Bejon, F. Luciani, K. Kedzierska, R. A. Seder, F. M. Ndungu, I.
925 A. Cockburn, Atypical B cells are part of an alternative lineage of B cells that participates
926 in responses to vaccination and infection in humans. *Cell Rep* **34**, 108684 (2021).
927 4. C. Sundling, C. Ronnberg, V. Yman, M. Asghar, P. Jahnmatz, T. Lakshmikanth, Y.
928 Chen, J. Mikes, M. N. Forsell, K. Sonden, A. Achour, P. Brodin, K. E. Persson, A.
929 Farnert, B cell profiling in malaria reveals expansion and remodelling of CD11c+ B cell
930 subsets. *JCI Insight* **5**, (2019).
931 5. S. Moir, J. Ho, A. Malaspina, W. Wang, A. C. DiPoto, M. A. O'Shea, G. Roby, S. Kottilil,
932 J. Arthos, M. A. Proschan, T. W. Chun, A. S. Fauci, Evidence for HIV-associated B cell
933 exhaustion in a dysfunctional memory B cell compartment in HIV-infected viremic
934 individuals. *J Exp Med* **205**, 1797-1805 (2008).
935 6. G. E. Weiss, P. D. Crompton, S. Li, L. A. Walsh, S. Moir, B. Traore, K. Kayentao, A.
936 Ongoiba, O. K. Doumbo, S. K. Pierce, Atypical memory B cells are greatly expanded in
937 individuals living in a malaria-endemic area. *J Immunol* **183**, 2176-2182 (2009).
938 7. C. Wei, J. Anolik, A. Cappione, B. Zheng, A. Pugh-Bernard, J. Brooks, E. H. Lee, E. C.
939 Milner, I. Sanz, A new population of cells lacking expression of CD27 represents a

940 notable component of the B cell memory compartment in systemic lupus erythematosus.
941 *J Immunol* **178**, 6624-6633 (2007).
942 8. I. Isnardi, Y. S. Ng, L. Menard, G. Meyers, D. Saadoun, I. Srdanovic, J. Samuels, J.
943 Berman, J. H. Buckner, C. Cunningham-Rundles, E. Meffre, Complement receptor
944 2/CD21- human naive B cells contain mostly autoreactive unresponsive clones. *Blood*
945 **115**, 5026-5036 (2010).
946 9. S. A. Jenks, K. S. Cashman, E. Zumaquero, U. M. Marigorta, A. V. Patel, X. Wang, D.
947 Tomar, M. C. Woodruff, Z. Simon, R. Bugrovsky, E. L. Blalock, C. D. Scharer, C. M.
948 Tipton, C. Wei, S. S. Lim, M. Petri, T. B. Niewold, J. H. Anolik, G. Gibson, F. E. Lee, J.
949 M. Boss, F. E. Lund, I. Sanz, Distinct Effector B Cells Induced by Unregulated Toll-like
950 Receptor 7 Contribute to Pathogenic Responses in Systemic Lupus Erythematosus.
951 *Immunity* **49**, 725-739 e726 (2018).
952 10. R. T. Sullivan, C. C. Kim, M. F. Fontana, M. E. Feeney, P. Jagannathan, M. J. Boyle, C.
953 J. Drakeley, I. Ssewanyana, F. Nankya, H. Mayanja-Kizza, G. Dorsey, B. Greenhouse,
954 FCRL5 Delineates Functionally Impaired Memory B Cells Associated with Plasmodium
955 falciparum Exposure. *PLoS Pathog* **11**, e1004894 (2015).
956 11. P. Holla, B. Dizon, A. A. Ambegaonkar, N. Rogel, E. Goldschmidt, A. K. Boddapati, H.
957 Sohn, D. Sturdevant, J. W. Austin, L. Kardava, L. Yuesheng, P. Liu, S. Moir, S. K.
958 Pierce, A. Madi, Shared transcriptional profiles of atypical B cells suggest common
959 drivers of expansion and function in malaria, HIV, and autoimmunity. *Sci Adv* **7**, (2021).
960 12. S. Portugal, C. M. Tipton, H. Sohn, Y. Kone, J. Wang, S. Li, J. Skinner, K. Virtaneva, D.
961 E. Sturdevant, S. F. Porcella, O. K. Doumbo, S. Doumbo, K. Kayentao, A. Ongoiba, B.
962 Traore, I. Sanz, S. K. Pierce, P. D. Crompton, Malaria-associated atypical memory B
963 cells exhibit markedly reduced B cell receptor signaling and effector function. *Elife* **4**,
964 (2015).
965 13. A. A. Ambegaonkar, K. Kwak, H. Sohn, J. Manzella-Lapeira, J. Brzostowski, S. K.
966 Pierce, Expression of inhibitory receptors by B cells in chronic human infectious
967 diseases restricts responses to membrane-associated antigens. *Sci Adv* **6**, eaba6493
968 (2020).
969 14. E. Wing, C. Sutherland, K. Miles, D. Gray, C. Goodyear, T. D. Otto, S. Breusch, G. J. M.
970 Cowan, M. Gray, A comprehensive analysis of rheumatoid arthritis B cells reveals the
971 importance of CD11c^{+ve} double-negative-2 B cells as the major synovial
972 plasma cell precursor. *bioRxiv*, 2023.2002.2015.526468 (2023).
973 15. M. F. Muellenbeck, B. Ueberheide, B. Amulic, A. Epp, D. Fenyo, C. E. Busse, M. Esen,
974 M. Theisen, B. Mordmuller, H. Wardemann, Atypical and classical memory B cells
975 produce Plasmodium falciparum neutralizing antibodies. *J Exp Med* **210**, 389-399
976 (2013).
977 16. P. Holla, A. Ambegaonkar, H. Sohn, S. K. Pierce, Exhaustion may not be in the human B
978 cell vocabulary, at least not in malaria. *Immunol Rev* **292**, 139-148 (2019).
979 17. C. S. Hopp, J. Skinner, S. L. Anzick, C. M. Tipton, M. E. Peterson, S. Li, S. Doumbo, K.
980 Kayentao, A. Ongoiba, C. Martens, B. Traore, P. D. Crompton, Atypical B cells up-
981 regulate costimulatory molecules during malaria and secrete antibodies with T follicular
982 helper cell support. *Sci Immunol* **7**, eabn1250 (2022).
983 18. A. E. Braddom, G. Batugedara, S. Bol, E. M. Bunnik, Potential functions of atypical
984 memory B cells in Plasmodium-exposed individuals. *Int J Parasitol* **50**, 1033-1042
985 (2020).
986 19. C. M. Andrade, H. Fleckenstein, R. Thomson-Luque, S. Doumbo, N. F. Lima, C.
987 Anderson, J. Hibbert, C. S. Hopp, T. M. Tran, S. Li, M. Niangaly, H. Cisse, D. Doumtabe,
988 J. Skinner, D. Sturdevant, S. Ricklefs, K. Virtaneva, M. Asghar, M. V. Homann, L.
989 Turner, J. Martins, E. L. Allman, M. E. N'Dri, V. Winkler, M. Llinas, C. Lavazec, C.
990 Martens, A. Farnert, K. Kayentao, A. Ongoiba, T. Lavstsen, N. S. Osorio, T. D. Otto, M.

991 Recker, B. Traore, P. D. Crompton, S. Portugal, Increased circulation time of
992 Plasmodium falciparum underlies persistent asymptomatic infection in the dry season.
993 *Nat Med* **26**, 1929-1940 (2020).
994 20. A. Stewart, J. C. Ng, G. Wallis, V. Tsioligka, F. Fraternali, D. K. Dunn-Walters, Single-
995 Cell Transcriptomic Analyses Define Distinct Peripheral B Cell Subsets and Discrete
996 Development Pathways. *Front Immunol* **12**, 602539 (2021).
997 21. A. H. Ellebedy, K. J. Jackson, H. T. Kissick, H. I. Nakaya, C. W. Davis, K. M. Roskin, A.
998 K. McElroy, C. M. Oshansky, R. Elbein, S. Thomas, G. M. Lyon, C. F. Spiropoulou, A. K.
999 Mehta, P. G. Thomas, S. D. Boyd, R. Ahmed, Defining antigen-specific plasmablast and
1000 memory B cell subsets in human blood after viral infection or vaccination. *Nat Immunol*
1001 **17**, 1226-1234 (2016).
1002 22. I. Sanz, C. Wei, S. A. Jenks, K. S. Cashman, C. Tipton, M. C. Woodruff, J. Hom, F. E.
1003 Lee, Challenges and Opportunities for Consistent Classification of Human B Cell and
1004 Plasma Cell Populations. *Front Immunol* **10**, 2458 (2019).
1005 23. A. E. Braddom, S. Bol, S. J. Gonzales, R. A. Reyes, K. Musinguzi, F. Nankya, I.
1006 Ssewanyana, B. Greenhouse, E. M. Bunnik, B Cell Receptor Repertoire Analysis in
1007 Malaria-Naive and Malaria-Experienced Individuals Reveals Unique Characteristics of
1008 Atypical Memory B Cells. *mSphere* **6**, e0072621 (2021).
1009 24. D. R. Glass, A. G. Tsai, J. P. Oliveria, F. J. Hartmann, S. C. Kimmey, A. A. Calderon, L.
1010 Borges, M. C. Glass, L. E. Wagar, M. M. Davis, S. C. Bendall, An Integrated Multi-omic
1011 Single-Cell Atlas of Human B Cell Identity. *Immunity* **53**, 217-232 e215 (2020).
1012 25. S. Gu, X. Han, C. Yao, H. Ding, J. Zhang, G. Hou, B. Qu, H. Zhou, Z. Ying, Z. Ye, J.
1013 Qian, Q. Guo, S. Chen, C. G. Vinuesa, D. Dai, N. Shen, The transcription factor Zeb2
1014 drives differentiation of age-associated B cells. *bioRxiv*, 2021.2007.2024.453633 (2021).
1015 26. X. Gao, Q. Shen, J. A. Roco, K. Frith, C. M. L. Munier, M. Nekrasov, B. Dalton, J.-S. He,
1016 R. Jaeger, M. C. Cook, J. J. Zaunders, I. A. Cockburn, ZEB2 regulates the development
1017 of CD11c+ atypical B cells. *bioRxiv*, 2022.2009.2001.506173 (2022).
1018 27. C. Akatsu, K. Shinagawa, N. Numoto, Z. Liu, A. K. Ucar, M. Aslam, S. Phoon, T. Adachi,
1019 K. Furukawa, N. Ito, T. Tsubata, CD72 negatively regulates B lymphocyte responses to
1020 the lupus-related endogenous toll-like receptor 7 ligand Sm/RNP. *J Exp Med* **213**, 2691-
1021 2706 (2016).
1022 28. C. Tan, R. Hiwa, J. L. Mueller, V. Vykunta, K. Hibiya, M. Noviski, J. Huizar, J. F. Brooks,
1023 J. Garcia, C. Heyn, Z. Li, A. Marson, J. Zikherman, NR4A nuclear receptors restrain B
1024 cell responses to antigen when second signals are absent or limiting. *Nat Immunol* **21**,
1025 1267-1279 (2020).
1026 29. C. Tan, J. L. Mueller, M. Noviski, J. Huizar, D. Lau, A. Dubinin, A. Molofsky, P. C.
1027 Wilson, J. Zikherman, Nur77 Links Chronic Antigen Stimulation to B Cell Tolerance by
1028 Restricting the Survival of Self-Reactive B Cells in the Periphery. *J Immunol* **202**, 2907-
1029 2923 (2019).
1030 30. J. Campisi, Aging, cellular senescence, and cancer. *Annu Rev Physiol* **75**, 685-705
1031 (2013).
1032 31. K. Contrepois, C. Coudereau, B. A. Benayoun, N. Schuler, P. F. Roux, O. Bischof, R.
1033 Courbeyrette, C. Carvalho, J. Y. Thuret, Z. Ma, C. Derbois, M. C. Nevers, H. Volland, C.
1034 E. Redon, W. M. Bonner, J. F. Deleuze, C. Wiel, D. Bernard, M. P. Snyder, C. E. Rube,
1035 R. Olaso, F. Fenaille, C. Mann, Histone variant H2A.J accumulates in senescent cells
1036 and promotes inflammatory gene expression. *Nat Commun* **8**, 14995 (2017).
1037 32. D. Frasca, M. Romero, A. Diaz, D. Garcia, S. Thaller, B. B. Blomberg, B Cells with a
1038 Senescent-Associated Secretory Phenotype Accumulate in the Adipose Tissue of
1039 Individuals with Obesity. *Int J Mol Sci* **22**, (2021).

1040 33. M. G. Giudizi, R. Biagiotti, F. Almerigogna, A. Alessi, A. Tiri, G. F. Del Prete, S. Ferrone,
1041 S. Romagnani, Role of HLA class I and class II antigens in activation and differentiation
1042 of B cells. *Cell Immunol* **108**, 97-108 (1987).
1043 34. J. G. Cyster, C. D. C. Allen, B Cell Responses: Cell Interaction Dynamics and Decisions.
1044 *Cell* **177**, 524-540 (2019).
1045 35. P. Stumptner-Cuvelette, P. Benaroch, Multiple roles of the invariant chain in MHC class
1046 II function. *Biochim Biophys Acta* **1542**, 1-13 (2002).
1047 36. R. Di Niro, S. J. Lee, J. A. Vander Heiden, R. A. Elsner, N. Trivedi, J. M. Bannock, N. T.
1048 Gupta, S. H. Kleinstein, F. Vigneault, T. J. Gilbert, E. Meffre, S. J. McSorley, M. J.
1049 Shlomchik, Salmonella Infection Drives Promiscuous B Cell Activation Followed by
1050 Extrafollicular Affinity Maturation. *Immunity* **43**, 120-131 (2015).
1051 37. V. Bergen, M. Lange, S. Peidli, F. A. Wolf, F. J. Theis, Generalizing RNA velocity to
1052 transient cell states through dynamical modeling. *Nat Biotechnol* **38**, 1408-1414 (2020).
1053 38. S. J. Gonzales, S. Bol, A. E. Braddom, R. Sullivan, R. A. Reyes, I. Ssewanyana, E.
1054 Eggers, B. Greenhouse, E. M. Bunnik, Longitudinal analysis of FcRL5 expression and
1055 clonal relationships among classical and atypical memory B cells following malaria.
1056 *Malar J* **20**, 435 (2021).
1057 39. U. Hershberg, E. T. Luning Prak, The analysis of clonal expansions in normal and
1058 autoimmune B cell repertoires. *Philos Trans R Soc Lond B Biol Sci* **370**, (2015).
1059 40. W. Meng, B. Zhang, G. W. Schwartz, A. M. Rosenfeld, D. Ren, J. J. C. Thome, D. J.
1060 Carpenter, N. Matsuoka, H. Lerner, A. L. Friedman, T. Granot, D. L. Farber, M. J.
1061 Shlomchik, U. Hershberg, E. T. Luning Prak, An atlas of B-cell clonal distribution in the
1062 human body. *Nat Biotechnol* **35**, 879-884 (2017).
1063 41. K. Zinszer, K. Charland, S. Vahey, D. Jahagirdar, J. C. Rek, E. Arinaitwe, J. Nankabirwa,
1064 K. Morrison, M. L. Sadoine, M. A. Tutt-Guerette, S. G. Staedke, M. R. Kamya, B.
1065 Greenhouse, I. Rodriguez-Barraquer, G. Dorsey, The Impact of Multiple Rounds of
1066 Indoor Residual Spraying on Malaria Incidence and Hemoglobin Levels in a High-
1067 Transmission Setting. *J Infect Dis* **221**, 304-312 (2020).
1068 42. M. R. Kamya, A. Kakuru, M. Muhindo, E. Arinaitwe, J. I. Nankabirwa, J. Rek, V. Bigira, J.
1069 Kapisi, H. Wanzira, J. Achan, P. Natureeba, A. Gasasira, D. Havlir, P. Jagannathan, P.
1070 J. Rosenthal, I. Rodriguez-Barraquer, G. Dorsey, The Impact of Control Interventions on
1071 Malaria Burden in Young Children in a Historically High-Transmission District of Uganda:
1072 A Pooled Analysis of Cohort Studies from 2007 to 2018. *Am J Trop Med Hyg* **103**, 785-
1073 792 (2020).
1074 43. S. J. Gonzales, K. N. Clarke, G. Batugedara, R. Garza, A. E. Braddom, R. A. Reyes, I.
1075 Ssewanyana, K. C. Garrison, G. C. Ippolito, B. Greenhouse, S. Bol, E. M. Bunnik, A
1076 Molecular Analysis of Memory B Cell and Antibody Responses Against Plasmodium
1077 falciparum Merozoite Surface Protein 1 in Children and Adults From Uganda. *Front*
1078 *Immunol* **13**, 809264 (2022).
1079 44. R. A. Reyes, K. Clarke, S. J. Gonzales, A. M. Cantwell, R. Garza, G. Catano, R. E.
1080 Tragus, T. F. Patterson, S. Bol, E. M. Bunnik, SARS-CoV-2 spike-specific memory B
1081 cells express higher levels of T-bet and FcRL5 after non-severe COVID-19 as compared
1082 to severe disease. *PLoS One* **16**, e0261656 (2021).
1083 45. C. L. Holness, D. L. Simmons, Molecular cloning of CD68, a human macrophage marker
1084 related to lysosomal glycoproteins. *Blood* **81**, 1607-1613 (1993).
1085 46. E. Gottfried, L. A. Kunz-Schughart, A. Weber, M. Rehli, A. Peuker, A. Muller, M.
1086 Kastenberger, G. Brockhoff, R. Andreesen, M. Kreutz, Expression of CD68 in non-
1087 myeloid cell types. *Scand J Immunol* **67**, 453-463 (2008).
1088 47. C. S. Hopp, J. Skinner, S. L. Anzick, C. M. Tipton, M. E. Peterson, L. Shanping, S.
1089 Doumbo, K. Kayentao, A. Ongoiba, C. Martens, B. Traore, P. D. Crompton, Atypical B

1090 cells upregulate co-stimulatory molecules during malaria and secrete antibodies with T
1091 follicular helper cell support. *BioRxiv*, (2021).
1092 48. J. L. Johnson, R. L. Rosenthal, J. J. Knox, A. Myles, M. S. Naradikian, J. Madej, M.
1093 Kostiv, A. M. Rosenfeld, W. Meng, S. R. Christensen, S. E. Hensley, J. Yewdell, D. H.
1094 Canaday, J. Zhu, A. B. McDermott, Y. Dori, M. Itkin, E. J. Wherry, N. Pardi, D.
1095 Weissman, A. Naji, E. T. L. Prak, M. R. Betts, M. P. Cancro, The Transcription Factor T-
1096 bet Resolves Memory B Cell Subsets with Distinct Tissue Distributions and Antibody
1097 Specificities in Mice and Humans. *Immunity* **52**, 842-855 e846 (2020).
1098 49. J. R. Groom, A. D. Luster, CXCR3 ligands: redundant, collaborative and antagonistic
1099 functions. *Immunol Cell Biol* **89**, 207-215 (2011).
1100 50. J. R. Groom, A. D. Luster, CXCR3 in T cell function. *Exp Cell Res* **317**, 620-631 (2011).
1101 51. G. Fontanesi, P. Costa, R. Rotini, P. Pignedoli, Total P.C.A. knee arthroprosthesis. *Ital J*
1102 *Orthop Traumatol* **14**, 41-48 (1988).
1103 52. N. M. Weisel, S. M. Joachim, S. Smita, D. Callahan, R. A. Elsner, L. J. Conter, M.
1104 Chikina, D. L. Farber, F. J. Weisel, M. J. Shlomchik, Surface phenotypes of naive and
1105 memory B cells in mouse and human tissues. *Nat Immunol* **23**, 135-145 (2022).
1106 53. C. Gregoire, L. Spinelli, S. Villazala-Merino, L. Gil, M. P. Holgado, M. Moussa, C. Dong,
1107 A. Zarubica, M. Fallet, J. M. Navarro, B. Malissen, P. Milpied, M. Gaya, Viral infection
1108 engenders bona fide and bystander subsets of lung-resident memory B cells through a
1109 permissive mechanism. *Immunity* **55**, 1216-1233 e1219 (2022).
1110 54. B. Keller, V. Strohmeier, I. Harder, S. Unger, K. J. Payne, G. Andrieux, M. Boerries, P. T.
1111 Felixberger, J. J. M. Landry, A. Nieters, A. Rensing-Ehl, U. Salzer, N. Frede, S. Usadel,
1112 R. Elling, C. Speckmann, I. Hainmann, E. Ralph, K. Gilmour, M. W. J. Wentink, M. van
1113 der Burg, H. S. Kuehn, S. D. Rosenzweig, U. Kolsch, H. von Bernuth, P. Kaiser-
1114 Labusch, F. Gothe, S. Hambleton, A. D. Vlagea, A. Garcia Garcia, L. Alsina, G. Markelj,
1115 T. Avcin, J. Vasconcelos, M. Guedes, J. Y. Ding, C. L. Ku, B. Shadur, D. T. Avery, N.
1116 Venhoff, J. Thiel, H. Becker, L. Erazo-Borras, C. M. Trujillo-Vargas, J. L. Franco, C.
1117 Fieschi, S. Okada, P. E. Gray, G. Uzel, J. L. Casanova, M. Fliegauf, B. Grimbacher, H.
1118 Eibel, S. Ehl, R. E. Voll, M. Rizzi, P. Stepensky, V. Benes, C. S. Ma, C. Bossen, S. G.
1119 Tangye, K. Warnatz, The expansion of human T-bet(high)CD21(low) B cells is T cell
1120 dependent. *Sci Immunol* **6**, eabh0891 (2021).
1121 55. S. Wang, J. Wang, V. Kumar, J. L. Karnell, B. Naiman, P. S. Gross, S. Rahman, K.
1122 Zerrouki, R. Hanna, C. Morehouse, N. Holoweckyj, H. Liu, T. Autoimmunity Molecular
1123 Medicine, Z. Manna, R. Goldbach-Mansky, S. Hasni, R. Siegel, M. Sanjuan, K.
1124 Streicher, M. P. Cancro, R. Kolbeck, R. Ettinger, IL-21 drives expansion and plasma cell
1125 differentiation of autoreactive CD11c(hi)T-bet(+) B cells in SLE. *Nat Commun* **9**, 1758
1126 (2018).
1127 56. M. Kilama, D. L. Smith, R. Hutchinson, R. Kigozi, A. Yeka, G. Lavoy, M. R. Kamya, S. G.
1128 Staedke, M. J. Donnelly, C. Drakeley, B. Greenhouse, G. Dorsey, S. W. Lindsay,
1129 Estimating the annual entomological inoculation rate for Plasmodium falciparum
1130 transmitted by Anopheles gambiae s.l. using three sampling methods in three sites in
1131 Uganda. *Malar J* **13**, 111 (2014).
1132 57. M. R. Kamya, E. Arinaitwe, H. Wanzira, A. Katureebe, C. Barusya, S. P. Kigozi, M.
1133 Kilama, A. J. Tatem, P. J. Rosenthal, C. Drakeley, S. W. Lindsay, S. G. Staedke, D. L.
1134 Smith, B. Greenhouse, G. Dorsey, Malaria transmission, infection, and disease at three
1135 sites with varied transmission intensity in Uganda: implications for malaria control. *Am J*
1136 *Trop Med Hyg* **92**, 903-912 (2015).
1137 58. N. T. Gupta, J. A. Vander Heiden, M. Uduman, D. Gadala-Maria, G. Yaari, S. H.
1138 Kleinstein, Change-O: a toolkit for analyzing large-scale B cell immunoglobulin repertoire
1139 sequencing data. *Bioinformatics* **31**, 3356-3358 (2015).

1140 59. E. Chichin, Community care for the frail elderly: the case of non-professional home care
1141 workers. *Women Health* **14**, 93-104 (1988).
1142 60. G. La Manno, R. Soldatov, A. Zeisel, E. Braun, H. Hochgerner, V. Petukhov, K.
1143 Lidschreiber, M. E. Kastriti, P. Lonnerberg, A. Furlan, J. Fan, L. E. Borm, Z. Liu, D. van
1144 Bruggen, J. Guo, X. He, R. Barker, E. Sundstrom, G. Castelo-Branco, P. Cramer, I.
1145 Adameyko, S. Linnarsson, P. V. Kharchenko, RNA velocity of single cells. *Nature* **560**,
1146 494-498 (2018).
1147 61. S. Van Gassen, B. Callebaut, M. J. Van Helden, B. N. Lambrecht, P. Demeester, T.
1148 Dhaene, Y. Saeys, FlowSOM: Using self-organizing maps for visualization and
1149 interpretation of cytometry data. *Cytometry A* **87**, 636-645 (2015).

1150

1151 **Acknowledgements**

1152 This work was supported by the National Institutes of Health (R01 AI153425 to EMB, R35
1153 GM128938 to FA, F31 AI169993 to RAR, TL1 TR002647 to RAR, T32 AI138944 to ABR, U19
1154 AI150741 to BG and PJ, and U19 AI089674). The authors acknowledge the Cell Analysis Core
1155 Facility (Dr. Sandra Cardona) and the Genomics Research Core Facility (Sean Vargas) at the
1156 University of Texas at San Antonio for support during this work. Data were generated in the
1157 Genome Sequencing Facility, which is supported by UT Health San Antonio, NIH-NCI P30
1158 CA054174 (Mays Cancer Center at UT Health San Antonio), and NIH Shared Instrument grant
1159 1S10OD030311-01 (S10 grant towards NovaSeq6000 sequencing system) and in the Flow
1160 Cytometry Shared Resource Facility, which is supported by UT Health San Antonio, NIH-NCI
1161 P30 CA054174 (Mays Cancer Center at UT Health), CPRIT (RP210126) and NIH Shared
1162 Instrument grant 1S10OD030432-01 (S10 grant towards the purchase of a DB FACSAria
1163 Fusion). Plasmids encoding 3D7 MSP1-bio, AMA1-bio, and BirA, were a kind gift from Dr. Gavin
1164 Wright (Wellcome Sanger Institute; Addgene plasmids #47709, 47741, and 32408).

1165

1166 **Author contributions**

1167 GB performed single-cell sequencing experiments and data analysis. RAR performed bulk RNA-
1168 sequencing experiments, spectral flow cytometry experiments, *in vitro* B cell cultures, ELISAs
1169 and data analysis. PD and FA analyzed single-cell sequencing data. ABR analyzed somatic
1170 hypermutation data. RG provided critical feedback on the manuscript. IS, PJ, MEF, and BG
1171 provided clinical samples. RAR, GB, SB, and EMB wrote the manuscript with input from all other
1172 co-authors. All authors contributed to the article and approved the submitted version.

1173

1174 **Competing interests**

1175 The authors declare that they have no competing interests.

1176

1177 **Data availability**

1178 All sequencing files will be available from the NCBI Sequencing Read Archive under BioProject
1179 accession no. TBD.

1180